1983

Laminar-turbulent transition of a non-Newtonian jet.

Kurichi Ramaswamy. Kumar
University of Windsor

CANADIAN THESES ON MICROFICHE

I.S.B.N.

THESES CANADIENNES SUR MICROFICHE

National Library of Canada
Collections Development Branch

Canadian Theses on
Microfiche Service

Ottawa, Canada
K1A 0N4

Bibliothèque nationale du Canada
Direction du développement des collections

Service des thèses canadiennes
sur microfiche

NOTICE

The quality of this microfiche is heavily dependent upon the quality of the original thesis submitted for microfilming. Every effort has been made to ensure the highest quality of reproduction possible.

If pages are missing, contact the university which granted the degree.

Some pages may have indistinct print especially if the original pages were typed with a poor typewriter ribbon or if the university sent us a poor photocopy.

Previously copyrighted materials (journal articles, published tests, etc.) are not filmed.

Reproduction in full or in part of this film is governed by the Canadian Copyright Act, R.S.C. 1970, c. C-30. Please read the authorization forms which accompany this thesis.

THIS DISSERTATION
HAS BEEN MICROFILMED
EXACTLY AS RECEIVED

AVIS

La qualité de cette microfiche dépend grandement de la qualité de la thèse soumise au microfilmage. Nous avons tout fait pour assurer une qualité supérieure de reproduction.

S'il manque des pages, veuillez communiquer avec l'université qui a conféré le grade.

La qualité d'impression de certaines pages peut laisser à désirer, surtout si les pages originales ont été dactylographiées à l'aide d'un ruban usé ou si l'université nous a fait parvenir une photocopie de mauvaise qualité.

Les documents qui font déjà l'objet d'un droit d'auteur (articles de revue, examens publiés, etc.) ne sont pas microfilmés.

La reproduction, même partielle, de ce microfilm est soumise à la Loi canadienne sur le droit d'auteur, SRC 1970, c. C-30. Veuillez prendre connaissance des formules d'autorisation qui accompagnent cette thèse.

LA THÈSE A ÉTÉ
MICROFILMÉE TELLE QUE
NOUS L'AVONS REÇUE

NL-339 (r. 82/08)

Canada

LAMINAR-TURBULENT TRANSITION OF A NON-NEWTONIAN JET

A THESIS

submitted to the Faculty of Graduate Studies through the Department of Mechanical Engineering in Partial Fulfillment of the Requirements for the Degree of Master of Applied Science at the University of Windsor

by

Kurichi Ramaswamy Kumar

Windsor, Ontario, Canada

1982

To my parents and sisters

ABSTRACT

The laminar length of a submerged jet of a non-Newtonian fluid is experimentally investigated. A flow visualization technique, which makes use of the birefringent property of the fluid and a circular polariscope, is employed to measure the laminar length. The experimental facility is also used as a "falling head" capillary viscometer. The laminar length data and the viscosity data are taken simultaneously.

Fluids of two different concentrations are studied. The results indicate that the concentration, hence the non-Newtonian nature of the fluid, has no influence on the laminar length of the jet for $600 < Re < 1100$. In the Reynolds number range of 50 to 200 the laminar length is affected by the viscous properties of the fluid. The results also indicate that there is not much difference in the laminar length of a Newtonian and non-Newtonian jet for $600 < Re < 1100$. The viscosity obtained from the present test facility is found to agree reasonably well with that obtained using a standard rotary viscometer.

ACKNOWLEDGEMENTS

The author wishes to express his deep and sincere gratitude to Drs. G.W. Rankin and K. Sridhar for their excellent guidance, unceasing help and generous aid during this study.

Thanks are due to Dr. Dekee for allowing the Rheomat viscometer to be available for the present study. The valuable suggestions of Dr. North, Dr. Dekee and Dr. McDonald are greatfully acknowledged.

Technical assistance rendered by Mr. R. Tattersall in constructing the test facility is greatfully acknowledged. Thanks are also due to Mrs. Carr for typing the manuscript.

The study was financially supported by Natural Sciences and Engineering Research Council of Canada through Grant Numbers A-2190 and A-1403.

TABLE OF CONTENTS

TABLE OF CONTENTS (CONT'D.)

LIST OF FIGURES

LIST OF TABLES

NOMENCLATURE

A	parameter in equation (B.13)
$A_0, A_1, A_2, \ldots A_{10}$	parameters in equation (B.14)
A_T	cross-sectional area of the downstream and upstream tanks
B	parameter in equation (B.13)
d	diameter of the capillary tube
g	gravitational constant = 9.81 m/s^2
h	head difference at any time t
K	consistency index of the fluids in the Power Law model
ℓ	length of the capillary tube
L	laminar length of the jet
m	slope of the ℓn h versus time curve, $\frac{d}{dt}(\ell n\ h)$; mass of the Mercury in equation 4.1
N_L	non-dimensional laminar length L/d
n	flow behaviour index of the fluid in the Power Law model
Q	flow rate through the capillary tube
R	radius of the capillary tube
Re	Reynolds Number, $Vd\rho/\eta$
S	parameter in equation (B.11), $\frac{\pi R^4 g}{8\ell A_T}$
t	time
V	average velocity in the capillary tube
W_n	uncertainty in a quantity n

$\dot{\gamma}_\omega$	shear rate at the wall
ε	sum of the errors squared
η	apparent viscosity
λ	wavelength
μ	dynamic viscosity
ρ	density
ρ_{Hg}	density of Mercury
τ_ω	wall shear stress
ϕ	apparent fluidity
ω_e, ω_o	extraordinary and ordinary index of refraction respectively

CHAPTER I

INTRODUCTION

1.1 Subject of Study

A submerged jet is formed when a fluid exits through a tube into a volume of the same fluid. In the present study the flow is fully developed and laminar at the tube exit. The jet continues to be laminar for some distance downstream of the tube exit. Beyond this distance the jet can become unstable causing transition to turbulent flow. The distance from the exit plane of the tube to the laminar to turbulent transition point is called the natural laminar length or simply laminar length. Figure 1.1 illustrates the various regions of a laminar-turbulent submerged jet.

Depending upon the Reynolds number in the tube, the jet may be any one of the following types:

(a) Fully laminar jet

(b) Laminar-turbulent jet

(c) Fully turbulent jet.

The present work is concerned with laminar-turbulent and fully laminar jets. In the case of a fully laminar jet the laminar length is the length after which the jet diffuses completely into the surrounding fluid without becoming turbulent.

This thesis presents an experimental investigation of the natural laminar length of an axisymmetric, submerged, non-Newtonian jet. Of particular interest is the effect that the concentration of the non-Newtonian fluid has on the laminar length. The non-

Newtonian fluid is prepared by mixing an organic dye powder in distilled water. The dye powder is commercially known as Milling Yellow and is supplied by Keystone Aniline & Chemicals Co., Chicago, Illinois, U.S.A. A flow visualization technique, which makes use of the birefringent characteristic of the fluid, is employed to measure the laminar length of the jet. The experimental facility allows simultaneous measurement of the viscosity of the fluid and the laminar length of the jet. The viscosity is determined using the test facility as a "falling head" capillary viscometer in conjunction with a non-linear parameter estimation technique. Laminar length measurements are taken using a displacement transducer and digital read-out unit.

1.2 Significance

One area in which the submerged jet finds an application is in the operation of fluidic devices such as the turbulence amplifier. Both a laminar-turbulent and fully laminar jet are essential for the proper functioning of this device. For a successful design, information concerning the stability of the jet is required. A number of current or potential applications of the turbulence amplifier require operation with non-Newtonian fluids. Most of the fluids encountered in the chemical industry, petroleum industry, food processing plants and many biological fluids are non-Newtonian in nature. It is speculated, in the literature, that the non-Newtonian behaviour of the fluid may affect the laminar length of the jet and hence the operation of the turbulence amplifier. Information on the variation of laminar length with Reynolds number will help the designer to determine the feasibility

and proper operation of such devices. The present study provides this information.

Research papers on non-Newtonian jets, particularly those concerning experimental investigations, are limited in number. It is expected that the results of the present study will be of some help to researchers attempting to achieve a basic understanding of non-Newtonian jets.

1.3 Aims

The main objectives of the present study are

(a) to investigate the variation of the laminar length of a submerged, axisymmetric jet of non-Newtonian fluid as a function of Reynolds number and its concentration, by using a birefringent flow visualization technique and also to make comparisons with previous Newtonian studies.

(b) to obtain the variation of the viscosity of the non-Newtonian fluid with shear rate, concurrently with the laminar length measurements using a non-linear parameter estimation technique in conjunction with a "falling head" capillary viscometer procedure.

CHAPTER II

LITERATURE SURVEY

The literature covered in this survey can be grouped into three major areas. These are:

(a) Non-Newtonian jets

(b) Laminar length measurements

(c) Characteristics of the fluid selected.

Each one is considered separately in what follows.

2.1 Non-Newtonian Jets

Most of the literature covered in this survey is concerned with solving the momentum equation to obtain the jet velocity profiles. Although this topic is not directly related to the present investigation it helps one to understand the basic behaviour of non-Newtonian jets. The literature cited below is predominantly concerned with laminar, incompressible, isothermal, submerged, non-Newtonian jets of a pseudo-plastic fluid.

Kapur (7) obtained a closed form similarity solution for the case of a two dimensional, incompressible jet of a power law fluid based on boundary layer assumptions. The closed form solution contained implicit functions for velocities and was expressed in terms of the axial distance x, the nondimensional velocity function $f'(n)$, the flow behaviour index n and consistency index K of the fluid. The special cases of $n < 1/2$, $n = 1/2$ and $n = 1/3$ were also considered separately. It was shown that the volume rate of discharge increases with axial distance.

Gutfinger and Shinnar (4), using a power law viscosity model,

obtained a complete analytical solution, similar to Kapur's, for a two dimensional, liquid into liquid jet. An analysis of the validity of the boundary layer assumptions was also performed. Using flow visualization techniques, they experimentally determined the velocity profiles. In both the Newtonian and non-Newtonian cases studied the agreement between theoretical and experimental velocity profiles was reasonable. The differences could have been due to the method they employed to measure the velocity profiles. During their experiment it was noticed that when the kinematic momentum of the non-Newtonian jet was equal to 1500 $m\ell/s^2$ the jet immediately spread to the sides and no clearly defined jet could be seen. They were not able to explain this phenomena.

Lemieux and Unny (8) obtained a numerical solution for a two dimensional, pseudoplastic, free jet by using a power law model. An empirical relation for the width of the jet was found to be

$$b = (\text{constant})\ x^{2/3n} \qquad (2.1)$$

It can be seen that the jet boundaries are linear when $n = 2/3$, concave for $n > 2/3$ and convex for $n < 2/3$. The authors reasoned that, because the non-dimensional velocity, $F'(\xi)$, tends to zero as the non-dimensional radial distance approaches infinity, the non-dimensional stream function, $F(\xi)$, should tend to a finite value. Later this was proven to be incorrect by Atkinson (1). In his analytical solution it was shown that $F'(\xi)$ tends to infinity as ξ tends to infinity.

Serth (19) obtained a numerical solution for an axisymmetric free laminar jet of a power law fluid with $n > 1/2$. Experimental velocity profiles using Separan AP30 having values of $n = 0.57$ and $K = 1.25$ dyne sec/cm^2 were also presented. A similar effect as that observed by Gutfinger and Shinnar was also noted in this study. A sharp drop in the velocity occurred as the jet came out of the orifice due to the expansion of the jet. Theoretical predictions failed in this region, however, at some distance away from the exit, the theoretical predictions were in good agreement. It was also shown that the axial velocity decay was proportional to $x^{1/(2n-1)}$.

Nystrom et al. (15) have provided an extensive review on mixing and drag reduction in non-Newtonian jets. It was shown, using the similarity principle, that for a turbulent jet there was no distinction in the gross characteristics between the Newtonian and non-Newtonian cases. Their experiments with POLYOX WSR-301 also supported this conclusion. In view of the fact that they used a fluid which had a flow behaviour index very close to unity ($n = 0.9$) differences between the Newtonian and non-Newtonian jet may not have been appreciable. The use of a probe to measure the velocity profiles may have introduced some errors. Further experiments using fluids having a much lower value of flow behaviour index and employing non-invasive techniques for velocity measurement are needed to confirm their conclusion.

Mitwally (14) obtained numerical solutions for an axisymmetric jet of non-Newtonian power law fluids. Solutions for plane and radial wall jets were also given. The governing non-linear partial differen-

tial equations were reduced to ordinary differential equations by suitable transformations and then solved numerically. One of the main conclusions is that a pseudoplastic fluid with $0.5 < n < 1$ starting as a laminar jet, will continue to be laminar further downstream. This is expected due to the prediction that the jet Reynolds number decreases with axial distance.

2.2 Laminar Length Measurements

All of the research work cited below is concerned with experimental determination of the laminar length of Newtonian jets which are either compressible or incompressible.

McKenzie and Wall (12) studied the laminar length of a submerged jet in the Reynolds number range of 5 to 400 for both the compressible and incompressible cases. They used a birefringent liquid for the incompressible jet study and a Helium-Air combination for the compressible jet study. The empirical relationship proposed by them for the laminar length is

$$\frac{L}{d} = \frac{1000}{Re} \qquad (2.2)$$

Reynolds (18) observed the flow of a dyed water jet into a tank of water. He noticed five different modes of breakdown of the jet depending on the Reynolds number. He indicated them on a plot of laminar length versus Reynolds number.

McNaughton and Sinclair (13) investigated a water into water jet using a tracer solution. They photographed the tracer solution jet flowing into a water tank. They also studied the variation

of laminar length with jet chamber diameter and length. Their empirical relation is

$$\frac{L}{d} = (9.97 \times 10^{7})(Re^{-2.46})(\frac{D}{d})^{-0.48}\ (\frac{\ell}{d})^{0.74} \qquad (2.3)$$

for $500 < Re < 2000$; $3 < \ell/d < 8$ and $3 < D/d < 24$

Marsters (10) measured the laminar length of a carbon dioxide jet issuing into air using the Shadowgraph technique. Ethylene was also used as a jet gas. He used several combinations of supply tube material, length and diameter and proposed an empirical correlation between the laminar length and Reynolds number for $1000 < Re < 2400$ as

$$\frac{L}{d} = (10^{9})(Re^{-2.3}) \qquad (2.4)$$

Beatty and Markland (2) did a similar study and determined that the upstream conditions had no significant effect on the laminar length.

2.3 Properties of the Non-Newtonian Fluid

The non-Newtonian fluid selected for the present experiment is a dye solution which can be prepared by mixing Milling Yellow powder with boiling water. This survey is concerned with the birefringent property and with measurement of the viscosity of the Milling Yellow dye solution.

The first investigator to use Milling Yellow as a birefringent fluid was Prados (16). In his dissertation on the analysis of two dimensional laminar flows, he determined the velocity profiles from

the interference patterns after suitable optical calibration of the fluid. This fluid behaved essentially in a Newtonian manner as the maximum experimental shear rate encountered was about 10 sec^{-1}.

Hirsch (5) performed experiments in such a shear rate range that the fluid behaved in a non-Newtonian manner. He measured velocity profiles in a diverging duct using the birefringent flow visualization technique. His measured velocity profiles and theoretical velocity profiles agreed very well. He has also given a rigorous procedure for preparing the Milling Yellow solution.

Hui Pih (6) presented a review of the application of birefringent flow visualization technique in various flow situations. He also indicated the usefulness of Milling Yellow for birefringent studies.

Maron et al (9) described an accurate and convenient method of determining the flow curves of non-Newtonian fluids using a "falling head" capillary viscometer. In this method a driving fluid is used to force the non-Newtonian fluid through a capillary tube. The measurement of the height of the driving fluid column as a function of time leads to the determination of the flow curve.

Walawender and Chen (21) used a similar approach to obtain the viscosity of non-Newtonian fluids. The only difference in their method is that instead of using a different driving fluid, the test fluid flows through the capillary tube under its own head. Using non-linear curve fitting techniques an empirical relationship between the falling head and time was obtained and from this the viscosity was determined.

CHAPTER III

FLOW VISUALIZATION AND THE NON-NEWTONIAN FLUID

A brief explanation of the flow visualization technique employed in the present study and a discussion concerning the non-Newtonian behaviour of the Milling Yellow solution is presented in this chapter.

3.1 Flow Visualization

Flow visualization plays an important role in many fluid flow problems. These techniques can provide an image of the entire flow field, unlike other flow measuring instruments, which give only localized information. It is also possible with these techniques to obtain quantitative information about the flow situation without disturbing it.

One of the methods employed in visualizing the flow is called the double refraction or birefringent technique. Birefringence is present in both solids and liquids and is an optical characteristic of the medium which is described as follows. When a birefringent fluid is at rest, it is optically isotropic; that is the refractive index of the fluid is the same in all directions. As soon as it is set into motion, it becomes optically anisotropic. When a linearly polarized light ray is incident upon such a medium, it is divided or refracted into two linearly polarized light components with their planes of polarization perpendicular to each other. One of the rays is called the 'ordinary ray' and the other the 'extraordinary ray'. They travel through the medium at different velocities. When they leave the medium, a relative angular phase shift exists between them. This phase shift is given by

$$\Delta\theta = \frac{2\pi dm}{\lambda} (\omega_e - \omega_o) \qquad (3.1)$$

where dm is the thickness of the medium, λ is the wavelength of the light and ω_e and ω_o are the medium's extraordinary and ordinary index of refraction respectively. The difference in the refractive indices, $\omega_e - \omega_o$, is proportional to the difference of principal strains and hence to the difference of principal stresses. A polariscope is used to observe this phase difference. It provides an image of the stress distribution over the flow field. Depending on whether the light employed to make the stress pattern visible is circularly polarized or linearly polarized the polariscope is called a circular polariscope or a plane polariscope. The following explanation concerning the operation of a polariscope is limited only to a circular polariscope as it is the one used in the present study. Figure 3.1 illustrates the general arrangement of a circular polariscope.

The circular polariscope consists of a light source, polarizer, two quarter-wave plates and analyzer. In the "dark field" arrangement of a circular polariscope the polarization axis of the polarizer and the analyzer are crossed; that is oriented perpendicular to each other. The fast and slow axis of the two quarter-wave plates are also crossed and arranged in such a manner that they are at 45° with respect to the polarizer axis. The light coming from the source first passes through the polarizer. The linearly polarized light from the polarizer then passes through the first quarter-wave plate which splits it into two

orthogonal components. These two rays travel at different velocities and are retarded relative to one another by an amount $\lambda/4$ when they emerge from the quarter-wave plate. This produces circularly polarized light which enters the test chamber containing the birefringent fluid. Only the components of these two rays along the principal axes of the flow field emerge from the test chamber and have an additional relative phase shift. The second quarter-wave plate resolves these rays into two orthogonal components and introduces a relative retardation of $\lambda/4$ between the two rays opposite to that occurring in the first quarter-wave plate. The main objective of the second quarter-wave plate is to convert the circularly polarized light of the first quarter-wave plate to linearly polarized light. When the two rays emerge from the second quarter-wave plate they pass through the analyzer. The analyzer passes only the resultant of these two rays along its axis of polarization. A fringe pattern is produced when these two rays interfere along the analyzer axis.

Fringes do not appear in the flow field when it is stationary because of the absence of shear stresses. Once the flow is initiated, the flow field is subjected to the action of shear stresses and hence fringe patterns are visible. When white light is used as the source, the fringe pattern will appear as a series of coloured bands. When the light employed is monochromatic, the fringe pattern will be a series of dark bands. These dark fringes are called isochromates. Each fringe corresponds to a given value of shear stress.

Dark fringes also appear in the case of a plane polariscope employing a monochromatic light source. The fringe pattern may be composed

of both isochromates and isoclinics. Isoclinic fringes appear when the direction of the principal stresses coincides with the direction of polarization. In a circular polariscope only the isochromatic fringes appear and the isoclinics are eliminated.

Flow parameters such as velocity and shear rate can quantitatively be estimated from the interference fringe patterns obtained in an unknown flow situation after calibrating the given liquid under known shear stress conditions. In the present study the only quantitative measurement to be made is the length of the laminar jet which corresponds to the length of the "ordered" isochromatic fringe pattern. In a laminar-turbulent jet the fringe patterns are ordered and stationary in the laminar region whereas in the turbulent region the ordered pattern is broken up. Hence, irregular, non stationary patterns are formed. The distance from the jet exit to the point where the pattern is no longer regular and stationary is defined as the laminar length of the jet.

3.2 Non-Newtonian Fluids

Skelland (20) defines non-Newtonian fluids as those fluids for which the flow curve is not linear through the origin at a given temperature and pressure. The viscosity may be dependent on the shear rate or on the duration of the shear rate and the past history of the fluid.

Skelland (20) classifies non-Newtonian fluids into three major groups. They are

(a) Time-independent fluids

(b) Time-dependent fluids

(c) Viscoelastic fluids.

A time-independent fluid has the characteristic that the rate of shear depends only on the local shear stress whereas in a time-dependent fluid shear rate depends on the magnitude and duration of the shear stress as well as on the past history of the shear stress. Viscoelastic fluids exhibit the properties of both fluids and elastic solids. The fluid selected for the present study falls into the time-independent category and hence a brief explanation of the behaviour of such fluids will be given.

Milling Yellow falls into the group of time-independent substances which do not have yield stress. Figure 3.2 illustrates the flow curves of various types of time-independent fluids. There are two common types of fluids in this category. They are called pseudoplastic or dilatant depending on whether their viscosity decreases or increases with shear rate respectively. Milling Yellow is found to exhibit pseudoplastic behaviour. A typical viscosity curve of a Milling Yellow solution is given in Figure 3.3. Three distinct regions may be identified. In the low shear rate region, the fluid is Newtonian and the viscosity, η_0, remains nearly constant. The viscosity varies with shear rate in the intermediate region and again remains nearly constant, η_∞, in the high shear rate region. In the non-Newtonian region, which has a shear rate range of approximately 50 to 800 s^{-1}, the following equation is

found to fit the experimental data quite well

$$\tau = K(\dot{\gamma})^{n} \qquad (3.2)$$

This equation is referred to as the "Power law" viscosity model. The values of K and n depend upon the type of fluid and concentration. The value of n is always less than unity for pseudoplastic fluids and greater than unity for dilatant fluids.

CHAPTER IV

EXPERIMENTAL DETAILS

4.1 Introduction

This chapter describes the experimental facility that was constructed for the measurement of laminar length and viscosity. It also includes a description of the experimental procedure that was adopted. A discussion concerning the selection of the working fluid is also given.

4.2 Selection of Working Fluid

The working fluid selection was based on the following two criteria:

(1) It should be birefringent.

(2) It should exhibit time-independent non-Newtonian behaviour.

Milling Yellow satisfies both of these requirements. There are, of course, many other fluids such as Vanadium-pentoxide and Poly-isobutylene which satisfy the above two requirements. Milling Yellow also exhibits the following desirable properties which the other fluids do not.

(a) High optical sensitivity.

(b) Moderate viscosity.

(c) Stability in contact with most of the common construction materials.

(d) Relatively easy to prepare.

Milling Yellow was therefore selected as the working fluid. A detailed description concerning the preparation of the Milling Yellow solution is given in Appendix (A).

4.3 General Test Facility

Figure 4.1 shows a schematic diagram of the test facility constructed for this investigation.

4.3.1 Fluid Flow Unit

The fluid flow unit consisted of the upstream tank, supply tube, jet chamber and the downstream tank. The fluid flows from the upstream tank to the jet chamber through the supply tube. From the jet chamber it flows through plastic tubing to the downstream tank. A brief description of the details of each of the components in the fluid flow unit is given below.

The upstream tank was made of plexiglass. It was circular in cross section with an inner diameter of 152 mm, thickness of 5 mm and a length of 356 mm. It was fixed onto the main supporting frame and its position was not changed during the experiment.

The supply tube consisted of a capillary tube with a diameter of 1.42 mm. It was made of stainless steel and was 305 mm in length. The capillary tube was housed inside a larger diameter tube in order to maintain straightness. The supply tube was connected to the upstream tank by means of a bellmouth entrance. This ensured smooth entry of fluid from the upstream tank. The other end of the supply tube was fixed so that it was flush with the upper wall of the

jet chamber.

The jet chamber was square in cross section and also made of plexiglass. The inner dimensions of the chamber were 102 x 102 mm. The wall thickness and the length were 9 mm and 254 mm respectively. A bleed port was provided and used to remove any air trapped inside.

The axes of the upstream tank, supply tube and the jet chamber were all on the same line. To ensure this alignment, holes were drilled in the corners of the square flanges that were mounted on the end of the upstream tank and jet chamber. An Aluminium rod was inserted in each set of holes. Only when the upstream tank and jet chamber were in alignment could these rods pass through the holes and be fixed in place.

The downstream tank was similar, in its dimensions, to the upstream tank. It was connected to the jet chamber by means of a 2.90 m. long and 12.70 mm diameter plastic tubing. A valve was located underneath the downstream tank. Unlike the upstream tank, the position of the downstream tank was not fixed. Setting different elevations of this tank was required to cover the desired range of Reynolds number. It was always kept at a lower level than the upstream tank.

4.3.2 Instrumentation

The fluid in the upstream tank flows into the downstream tank when the flow is started. As the upstream and downstream tanks are identical in all dimensions, the drop in the level of liquid in one tank will be equal to the rise in the other. Hence it is sufficient to measure the liquid level in any one of the tanks. In order to determine the viscosity and the flowrate it was necessary to know only the time rate

of change of head and not the actual head. The method described below was used to measure this change in head..

A depth gauge and a simple electric circuit were used to measure the liquid level in the downstream tank. A thin copper rod, with a sharp tip, was fixed to a vernier scale. This unit was called the depth gauge and was mounted on the downstream tank. An electric circuit was formed consisting of a power supply, an indicator light, the copper rod, the downstream tank and the fluid in the tank. In order to measure the liquid level, first the copper rod was positioned so that it touched the surface of the fluid. This was done before the flow was started. Once the flow was initiated the vernier scale was moved up by a known distance so that the top of the copper rod was at a higher level than the level of the liquid. As the level of liquid in the downstream tank was increasing, after some time the surface of the liquid touched the top of the copper rod. As soon as this contact was made, the circuit was closed and current flowed which made the light go on. In this way the rise of liquid level at various instants of time, was measured. In order to determine the actual difference in the levels of the liquid at any time, it was sufficient to know the difference in the levels before the flow was started and the rise in the liquid level up to that time.

In order to measure the laminar length of the jet, a photographic technique was first attempted. Photographs of the fringe patterns were taken and then projected onto a large screen using a film strip projector. The intensity of the polarized light, which

made the fringes visible, was very low and hence the quality of the pictures was not good. To locate the transition point from these photographs was very difficult. The photographic method provided only a static view of the jet at a particular instant of time and did not give any information on the unsteady nature of the flow. Hence the photographic method was abandoned and a direct measurement technique employed. In this method the transition point could be easily located by identifying the intersection of the unsteady turbulent region and steady laminar region.

A displacement transducer and a digital read-out unit were employed to measure the laminar length. The main body of the transducer was mounted onto the side of the jet chamber. The "slider" of the transducer was fastened to a metal block which moved along a guideway. Two thin metallic wires were fixed to the guide block. Both wires were horizontal and parallel to each other, however, one was located in front of and one behind the jet chamber. They could be positioned along the length of the jet chamber and were parallel to the front and rear faces. In order to take a reading, the operator's eye was positioned in such a way that both wires were aligned and appeared to be a single wire. In this way the parallax error was eliminated. The digital read-out unit, which was connected to the transducer, gave the displacement of the wires from the exit of the capillary tube.

4.3.3 Polariscope

The polariscope used in the present study is shown in Figure

4.2. It consisted of a light source, a polarizer, two quarter-wave plates and an analyzer. It could be operated either as a plane polariscope or as a circular polariscope. In the present study it was operated as a dark field circular polariscope.

The light source consisted of a bank of six fluorescent tubes mounted behind a diffusing screen. This provided a uniform illumination over the entire flow field.

The polarizer and the first quarter-wave plate were mounted as a single unit. Similarly the second quarter-wave plate and the analyzer were mounted as a single unit. This distance between these two units was approximately 480 mm. The polarizer, the two quarter-wave plates and the analyzer were 203 mm in diameter.

4.3.4 Rheometer

The rheological behaviour of the Milling Yellow solution was determined with the aid of a rotary viscometer. Figure 4.3 is a photo of the Contraves Rheomat 30 viscometer that was used in the present study. It consisted of a bob rotating concentrically inside a cup. The cup and bob combination is referred to as the measuring system. Depending upon the viscosity of the fluid and the shear rate desired, the proper measuring system was selected. Measuring system A had a shear rate range of 8.99×10^{-2} to 662 sec^{-1} and was used in the present study. The shear rate was varied by changing the rotational speed of the bob.

4.3.5 Main Supporting Frame

The main supporting frame was made of mild steel 'L' sections.

The frame was rectangular in cross section (406 x 584 mm) and stood 1.5 m high. Cross bars along the length of the frame provided means to position the upstream tank at different heights. This frame was bolted rigidly to a laboratory table. The table was of solid construction and also supported the polariscope.

4.4 Experimental Procedure

In this section the procedures associated with the experimental determination of the laminar length and the viscosity are described in detail. The experimental procedure described below, excluding 4.4.2, was adopted for fluids of different concentrations.

4.4.1 Preparation of the Working Fluid

The first step in the experiment was to prepare a birefringent solution of Milling Yellow. Such a fluid was prepared using the detailed procedure given in Appendix (A).

4.4.2 Determination of the Diameter of the Capillary Tube

An accurate value of the diameter of the capillary tube was required to determine the viscosity of the fluid. Extreme care was taken to determine the diameter of the tube. Mercury was allowed to flow through the tube which eliminated any trapped air. The flow was then stopped and the excess Mercury at the inlet removed. The Mercury that remained inside the tube was then collected and weighed. The diameter of the tube was determined by using the equation

$$d = \left(\frac{4m}{\pi \ell \rho_{Hg}}\right)^{1/2} \qquad 4.1$$

where d and ℓ are the diameter and length of the tube respectively, m is the mass of the Mercury collected and ρ_{Hg} is the density of the Mercury at the test temperature.

4.4.3 Initial Setup Procedure

The fluid flow unit was mounted on the main supporting frame in such a way that the jet chamber was located midway between the analyzer and polarizer. The entire unit was mounted such that the capillary tube was vertical. After aligning the two faces of the jet chamber parallel to the quarter-wave plates, the unit was clamped rigidly to the frame. The downstream tank, which included the depth gauge assembly, was positioned at the desired elevation. The fluid was then introduced into the system. Care was taken to remove any air that was trapped inside the jet chamber.

The polarizer, two quarter-wave plates and analyzer were arranged to operate as a circular polariscope.

The digital read-out was initialized by positioning the two wires attached to the slider of the displacement transducer at the jet exit. The readout was then set to zero and the temperature of the fluid also recorded.

4.4.4 Laminar Length Measurements

The flow was initiated and a stopwatch started at the same instant. Even though white light was used for visualization only dark and light (yellow) fringes were visible in the flow field and the transition point could be clearly identified. Figure 4.4 is a photograph of the fringe pattern obtained for a laminar-turbulent jet.

The wire assembly connected to the transducer was then moved to coincide with this laminar to turbulent transition point. The reading on the digital read-out was recorded when the two wires appeared as a single wire when viewed through the analyzer. For each laminar length reading the corresponding time on the stopwatch was also noted.

4.4.5 Viscosity Measurements

It was necessary to know the head versus time relationship in order to determine the viscosity of the fluid using the experimental facility. The depth gauge and stopwatch readings were recorded simultaneously at approximately equal intervals of head for this purpose. The temperature of the fluid was also noted at regular intervals of time.

The viscosity of the fluid was also determined by using the Rheomat described in 4.3.4. The viscosity of a sample of the fluid at various shear rates was determined.

In order to cover the desired range of laminar length and viscosity it was necessary to perform the experiment with different elevation settings of the downstream tank.

The initial difference in the levels of liquid was relatively small for some downstream tank settings. The experimental time was very long using such settings. To minimize this time it was decided to reduce the diameter of the upstream and downstream tanks. This was accomplished by installing two smaller diameter tanks inside the original, larger diameter tanks. The new tanks were 356 mm in length and 50.8 mm in diameter. This reduced the experimental time considerably.

CHAPTER V

RESULTS AND DISCUSSION

The laminar length and viscosity data obtained in the present experimental study are presented in Tables 4. through 24. The results are discussed in detail in the following section.

5.1 Laminar Length of the Jet

The measured laminar length of the jet is non-dimensionalized by dividing it by the diameter of the supply tube. This is referred to as the laminar length, N_L. Tables 17 to 24 represent the laminar length data. For any particular head difference (and hence maximum shear rate) the Reynolds number represented in the table is calculated using the diameter of the tube, the average velocity in the tube and viscosity of the fluid.

Figure 5.1 illustrates the variation of laminar length, N_L, with Reynolds number, Re, for two different concentrations of the fluid. From the figure it can be seen that the laminar length increases in the Reynolds number range of 50 to 200. The variation of laminar length is different for the two concentrations. Very low intensity of the fringes in this range made it difficult to locate the exact point after which the jet completely diffused into the surrounding fluid. This is the reason for the scattering of the data for both concentrations. The laminar length data for both concentrations coalesce for $200 < Re < 350$. For Reynolds numbers greater than 350 and up to 600 , the laminar length of the jet was more than the diameter of the analyzer. Hence laminar length measurements could not be taken in this range. In the Reynolds number range of 600 to 700 of a laminar-turbulent jet, the data indicate

a sharp drop in the laminar length. In this range of Reynolds number, the laminar length was unsteady and fluctuated considerably and hence only the mean value of the fluctuations are shown in Figure 5.1. For Reynolds numbers greater than 700, the laminar length decreases less sharply with the Reynolds number.

From Figure 5.1 it can be seen that, for a laminar-turbulent jet ($600 < Re < 1100$) there is little difference in the variation of the laminar length with Reynolds number for the two concentrations. The lack of dependence of laminar length on the concentration (and hence on the rheological properties of the fluid) may be due to the fact that the turbulent stresses in the jet dominate over the viscous stresses. In the case of a fully laminar jet and in the Reynolds number range of 50 to 200, the variations of laminar length with Reynolds number are appreciably different for the two concentrations. This may be due to the fact that turbulent stresses are absent and the laminar length depends on parameters in addition to Reynolds number as defined here.

The variation laminar length with Reynolds number is correlated using a curve fitting technique for a Reynolds number range of 650 to 1000. The empirical relation obtained is

$$N_L = A\ Re^B \qquad (5.1)$$

where $A = 9.5 \times 10^7$

$B = -2.23$ and $\varepsilon = 0.1$

In Figure 5.2 the results of the present study are compared with some of the similar Newtonian studies. In the case of a laminar-turbulent jet ($600 < Re < 1100$) the present results compare well with

the results given by McNaughton and Sinclair [13] for liquid jets. The lack of agreement between the present results and those of McKenzie and Wall [12] could be attributed to the fact that their results were taken with jets which were neither axisymmetric nor free. The agreement of the present study with the results of Beatty and Markland [2] and with those of Marsters [10] is more reasonable than the agreement between the present study and Reference 12. The present data and Marster's [10] results show a good agreement in the slope of the plot of N_L vs Re. However the difference between the N_L values of the two studies cannot be explained by the uncertainty of the present data. We should also note that the results of Beatty and Markland [2] and Marters [10] were taken using gaseous jets. It can also be seen that in the case of fully laminar jets ($50 < Re < 350$) the present results do not compare well with those of Beatty and Markland [2]. As mentioned earlier, the reason could be that the non-Newtonian nature of the fluid influences the laminar length of a fully laminar jet and unlike the Newtonian jet, Reynolds number is not sufficient to collapse the data.

Mitwally [14] speculated, as mentioned in Chapter II, that when the flow behaviour index, n, of a pseudoplastic fluid is between 0.5 and 1 and if a submerged jet of this fluid begins as a laminar jet, the jet will never become turbulent. In the present experiment the fluid used was pseudoplastic in nature and the value of n was between 0.5 and 1. For $600 < Re < 1100$ it was observed that the jet indeed did become turbulent even though it was laminar at the exit of the tube. This shows that the instability of a submerged jet cannot be based upon

the variation of the local Reynolds number (in which n is the important parameter) as defined by Mitwally.

5.2 Viscosity Measurements

The experimental data obtained from the rotary viscometer (Rheomat) and from the present experimental facility are presented in Tables 2 through 16. The procedure that was used to determine the viscosity of the fluid from the head versus time data is given in Appendix (B).

The variation of viscosity with shear rate obtained from the rotary viscometer and from the present test facility using it as a capillary viscometer are given in Figures 5.3 and 5.4 for the two fluid concentrations used. The capillary viscometer is capable of yielding a continuous curve of the viscosity variation over a wide range of shear rates ($10 < \dot{\gamma} < 9000$). The agreement between the rotary viscometer results and the capillary viscometer results is reasonably good in trend only. At low shear rates ($0 < \dot{\gamma} < 20$) and at high shear rates ($500 < \dot{\gamma} < 660$) the viscosity values given by the rotary viscometer disagree with the capillary viscometer values. The reason for the disagreement could be that the relatively low viscosity of the fluid makes it unsuitable for testing with the rotary viscometer.

Even though the tests were conducted during a period of the day when the room temperature fluctuation was minimum, the variation of temperature between and during runs could not be avoided. This may be one of the reasons for the slight discontinuities in the viscosity curve. It is speculated that a better curve fitting technique would give a more continuous variation.

CHAPTER VI

CONCLUSIONS AND RECOMMENDATIONS

6.1 Conclusions

The variation of the laminar length with Reynolds number is experimentally obtained for a submerged, axisymmetric jet of a non-Newtonian fluid. From this information the following conclusions are made.

(a) The laminar length of a laminar-turbulent jet ($600 < Re < 1100$) is independent of the concentration and hence the non-Newtonian nature of the fluid.

(b) The non-Newtonian nature has a substantial effect on the laminar length of a fully laminar jet ($50 < Re < 200$).

(c) The present results compare well with the results of McNaughton and Sinclair [13] for laminar-turbulent liquid jets.

The variation of the viscosity of the non-Newtonian fluid with shear rate is obtained using the present test facility. The agreement between the rotary viscometer results and capillary viscometer results is reasonably good in trend only.

6.2 Recommendations

(1) Variation of the temperature of the fluid during tests should be minimized by using a temperature controlled bath.

(2) Further experiments should be performed to verify the conclusions of the present study, with few changes in the present experimental facility and with fluids having values of n less than 0.5.

(3) Further experiments could be carried out using different diameters of the supply tube and different sizes of test chamber to observe whether the laminar length is affected by these changes.

REFERENCES

1. Atkinson, C., "On the laminar two dimensional free jet of an incompressible pseudoplastic fluid", Journal of Applied Mechanics, December 1972. p. 1162-1164.

2. Beatty, E.K. and Markland, E., "Feasibility study of laminar jet deflection fluidic elements", C.F.C. (3), Paper H1.

3. Dally, J.W. and Riley, W.F., "Experimental stress analysis", McGraw-Hill, New York, 1978.

4. Gutfinger, C. and Shinnar, R., "Velocity distribution in two dimensional laminar liquid-into-liquid jets in power law fluids", A.I.Ch.E. Journal, Vol. 10, No. 5, September 1964, p. 631-635.

5. Hirsch, A.E., "The flow of a Non-Newtonian fluid in a diverging duct, Experimental", Doctoral dissertation, Chemical Engineering, University of Tennessee, 1964.

6. Hui Pih, "Birefringent fluid flow methods in Engineering", Experimental Mechanics, December 1980, p. 437-444.

7. Kapur, J.N., "On the two dimensional jet of an incompressible pseudo-plastic fluid", Journal of Physical Society of Japan, Vol. 17, No. 8, August 1962, p. 1303-1309.

8. Lemieux, P.F. and Unny, T.E., "The laminar two dimensional free jet of an incompressible pseudoplastic fluid", Journal of Applied Mechanics, December 1968, p. 810-812.

9. Maron, S.H., Kreiger, I.M. and Sisko, A.W., "A capillary viscometer with continuously varying pressure head", Journal of Applied Physics, Vol. 25, No. 8, August 1954, p. 971-976.

10. Marsters, G.F., "Some observations on the transition to turbulence in small unconfined free jets", Report No. 1-69, Dept. of Mech. Eng., Queen's University, Kingston, Ontario, Canada, October 1969.

11. McKenzie, C.P. and Dorsey, W.P., "Transition to turbulence for submerged incompressible and free compressible fluid jets", Report No. OR 8882, Martin Marietta Corporation, Orlando, Florida, June 1967.

12. McKenzie, C.P. and Wall, D.B., "Investigation of jet transition phenomena", Report No. OR 9442, Martin Marietta Corporation, Orlando, Florida, June 1968.

13. McNaughton, K.J. and Sinclair, C.G., "Submerged jets in short cylindrical flow vessels", Journal of Fluid Mechanics, Vol. 25, 1966, p. 367-375.

14. Mitwally, E.M., "Solutions of laminar jet flow problems for Non-Newtonian power law fluids", Journal of Fluids Engineering, Vol. 100, September, 1978, p. 363-366.

15. Nystrom, K.S., Bouscher, R.F. and Fillipson, L., "A review and an investigation concerning jets of Polyox and water in connection with the fluid mechanics of power fluidics", Technical Note AE-701, The Aeronautical Research Institute of Sweden, Stockholm, 1974.

16. Prados, J.W., "The analysis of two dimensional laminar flow utilizing a doubly refracting liquid", Doctoral dissertation, University of Tennessee, 1957.

17. Rankin, G.W., "Developing region of laminar jets", Doctoral dissertation, Mechanical Engineering, University of Windsor, 1980.

18. Reynolds, A.J., "Observation of a liquid-into-liquid jet", Journal of Fluid Mechanics, Vol. 14, 1962, p. 552-556.

19. Serth, R.W., "The axisymmetric free laminar jet of a power law fluid", Journal of Applied Mathematics and Physics, Vol. 23, 1972, p. 131-138.

20. Skelland, A.H.P., "Non-Newtonian flow and heat transfer", John Wiley & Sons, Inc., New York, 1967.

21. Walawender, W.P. and Chen, T.Y., "Flow curve determination for Non-Newtonian fluids", Chemical Engineering Education, Winter 1975, p. 10-15.

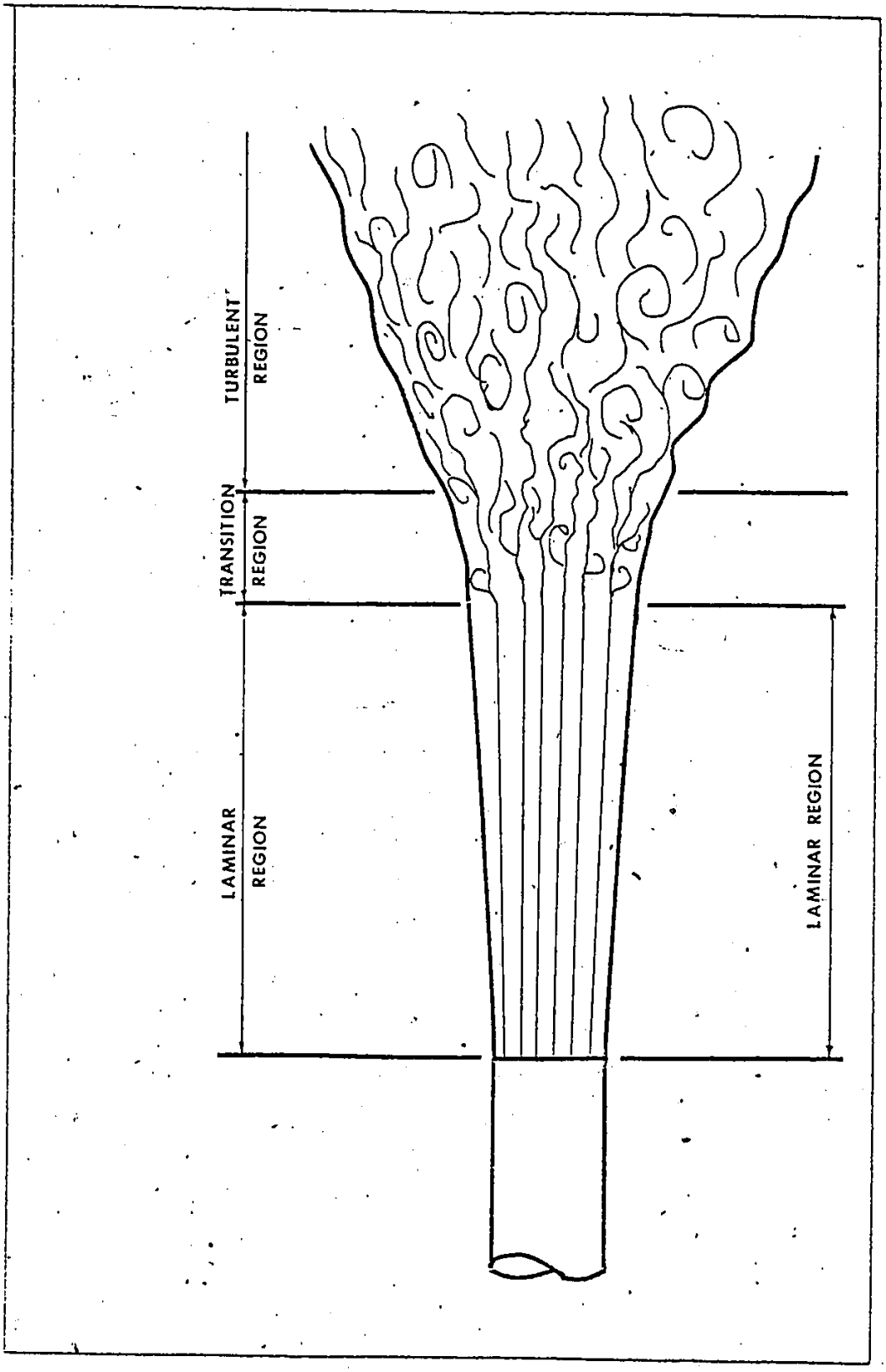

FIGURE 1.1 LAMINAR – TURBULENT SUBMERGED JET

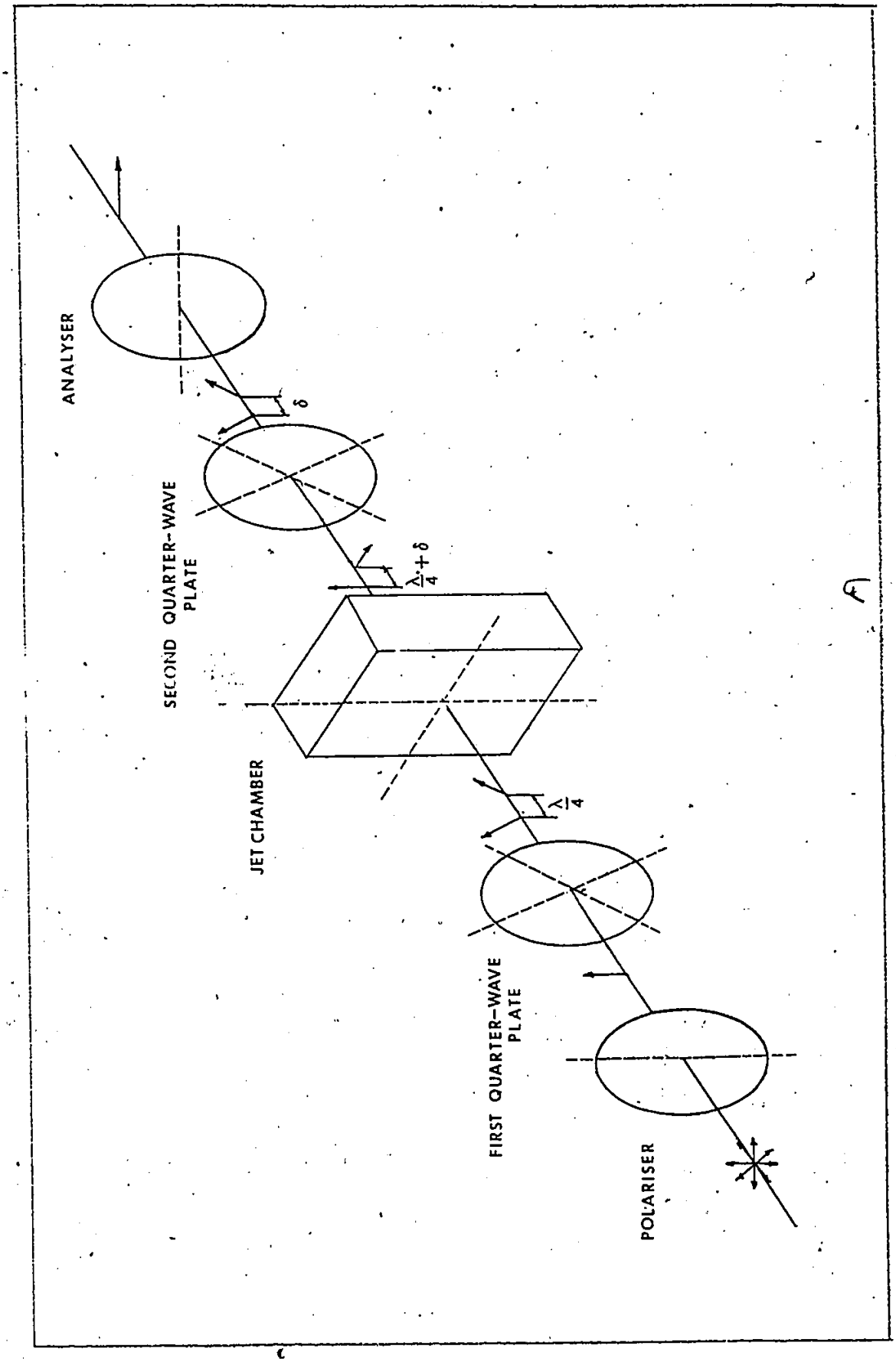

FIGURE 3.1 GENERAL ARRANGEMENT OF A CIRCULAR POLARISCOPE

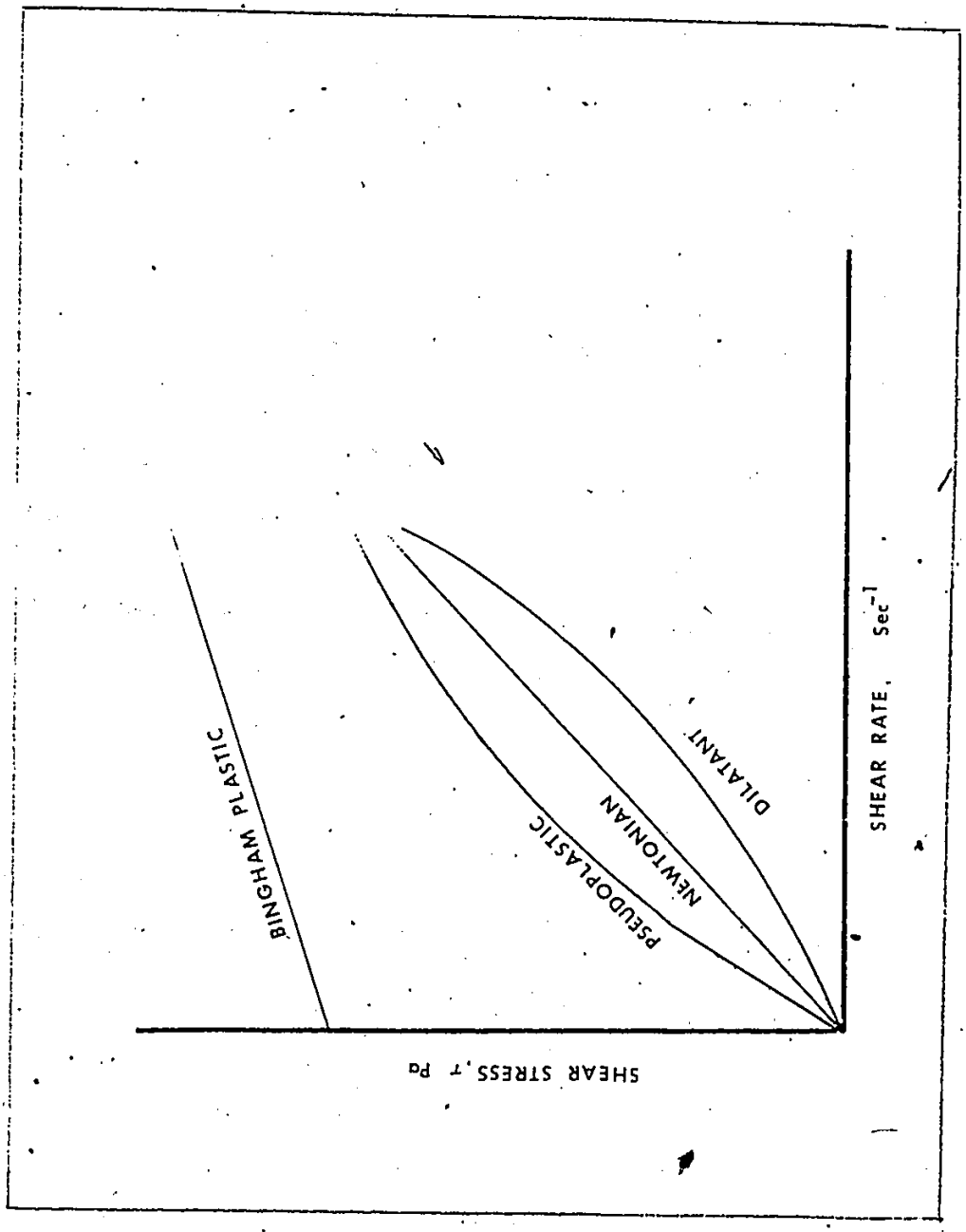

FIGURE 3.2 TIME-INDEPENDENT FLUIDS

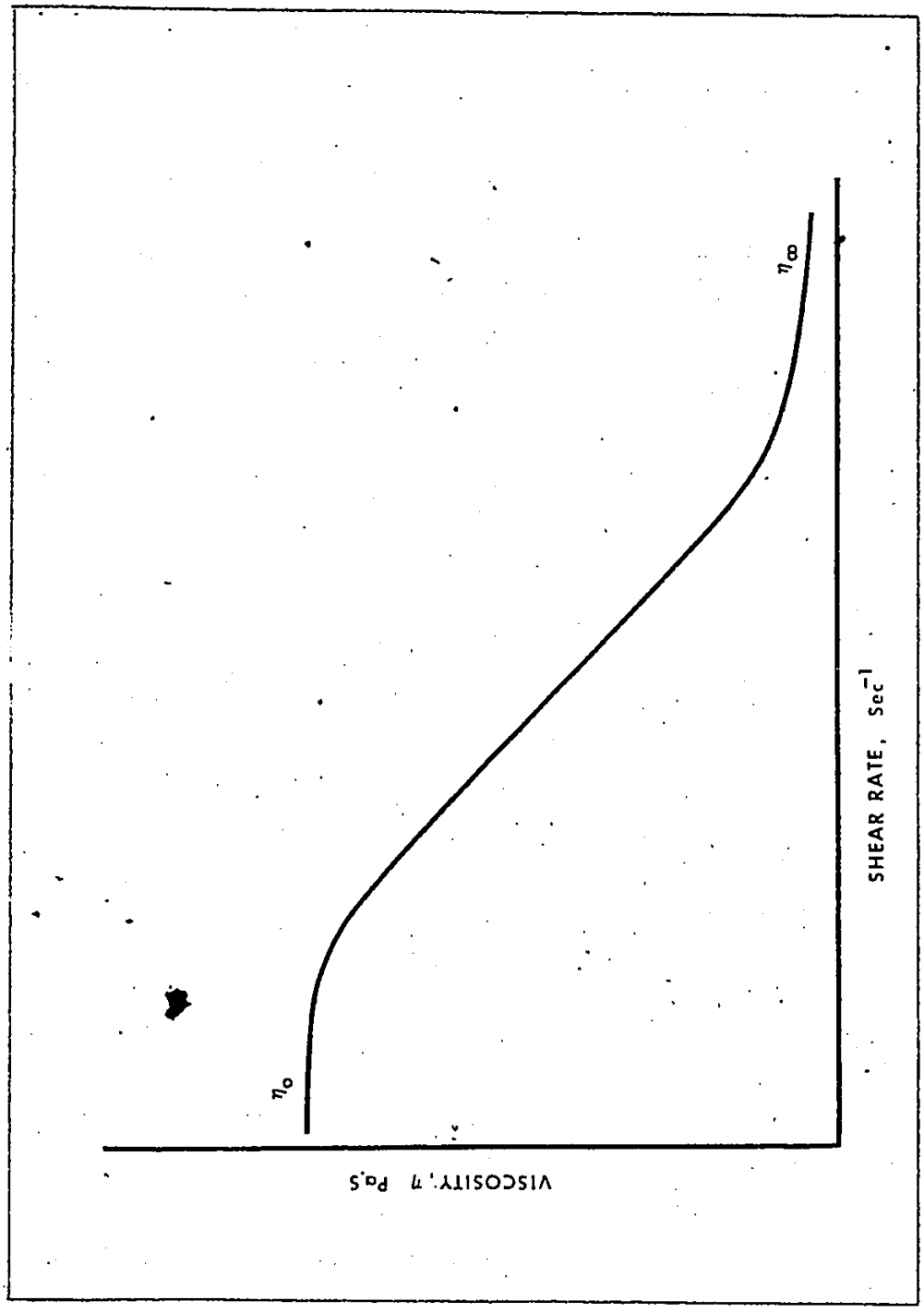

FIGURE 3.3 TYPICAL VISCOSITY DIAGRAM FOR MILLING YELLOW

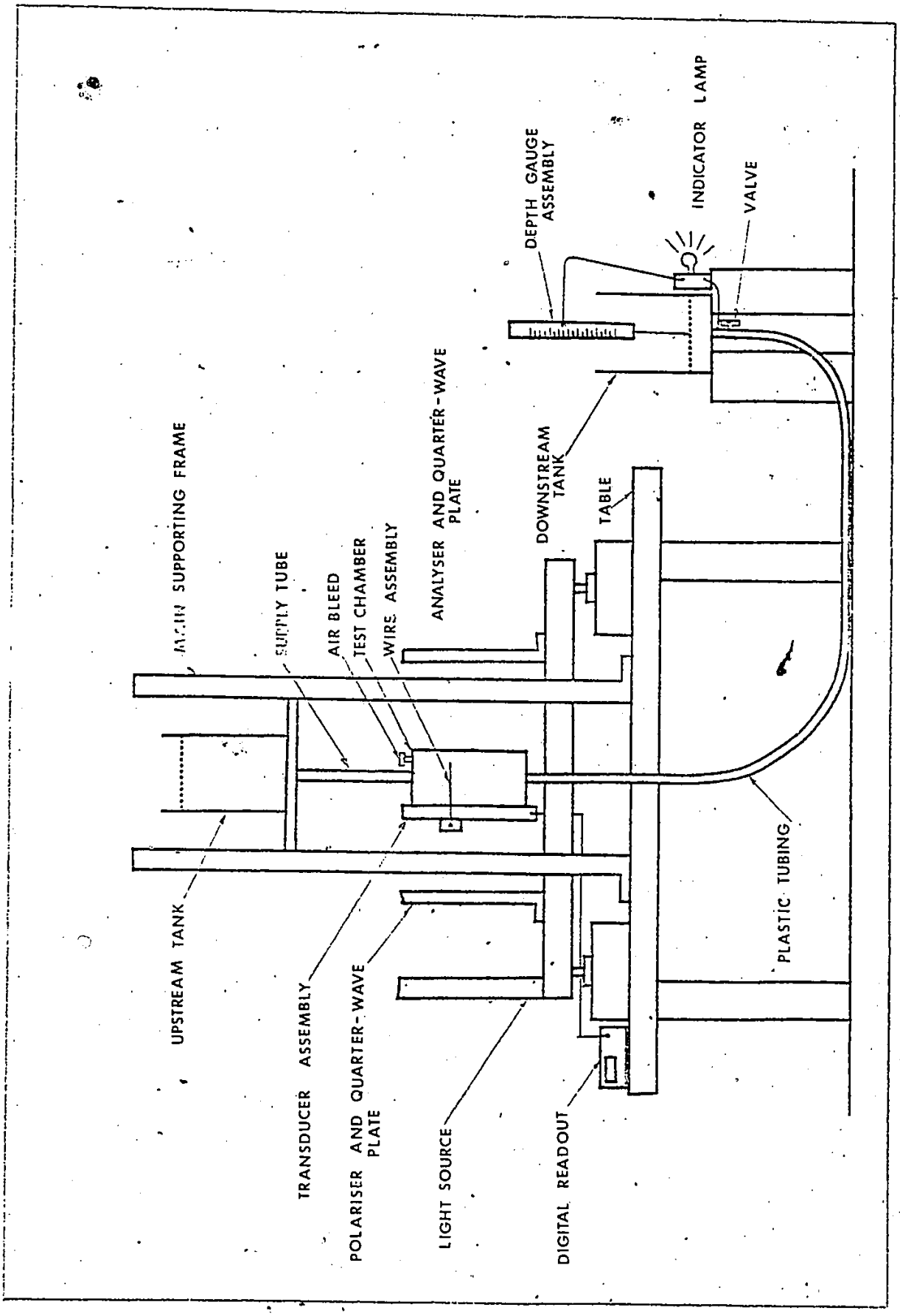

FIGURE 4.1 GENERAL TEST FACILITY

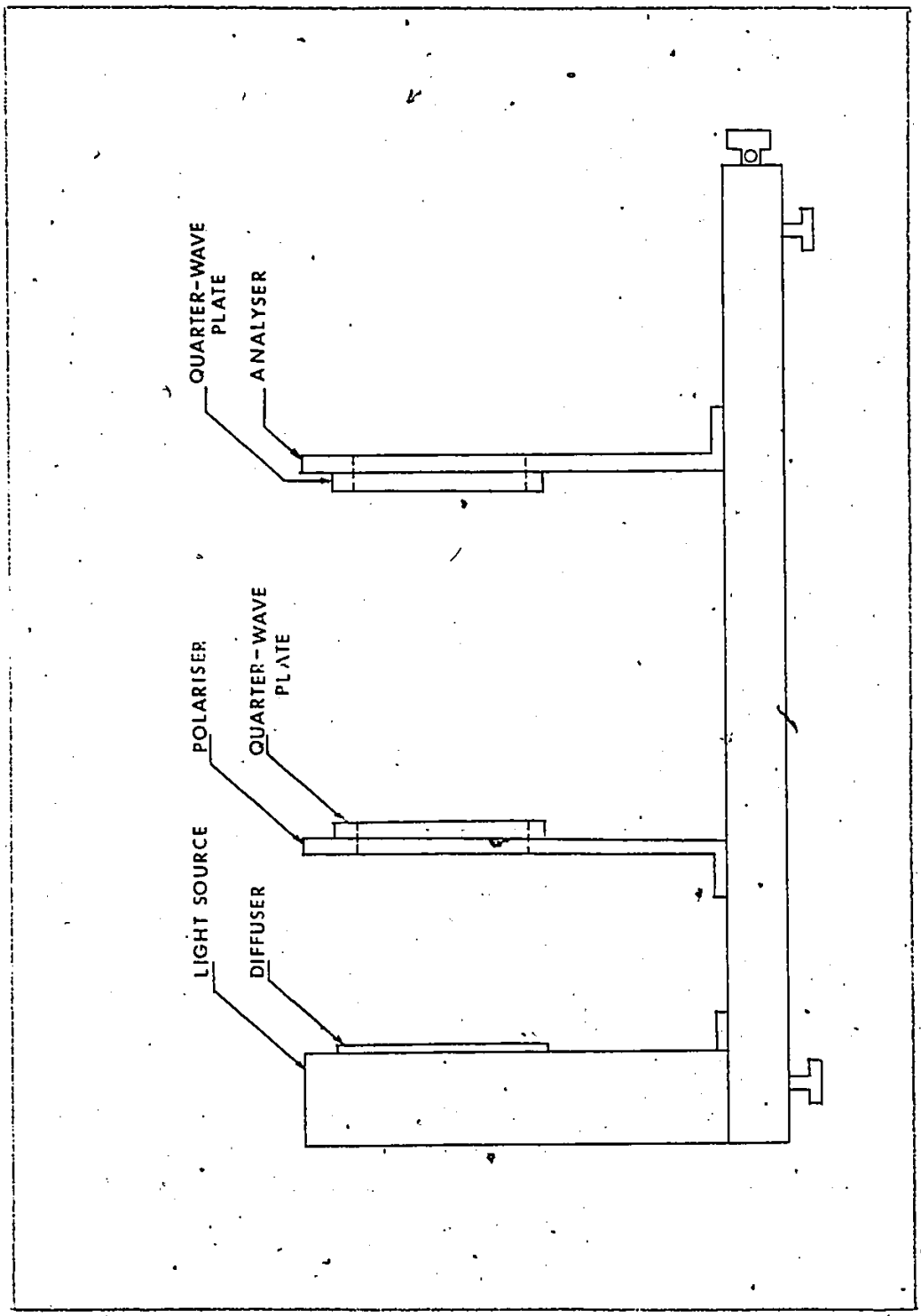

FIGURE 4.2 POLARISCOPE

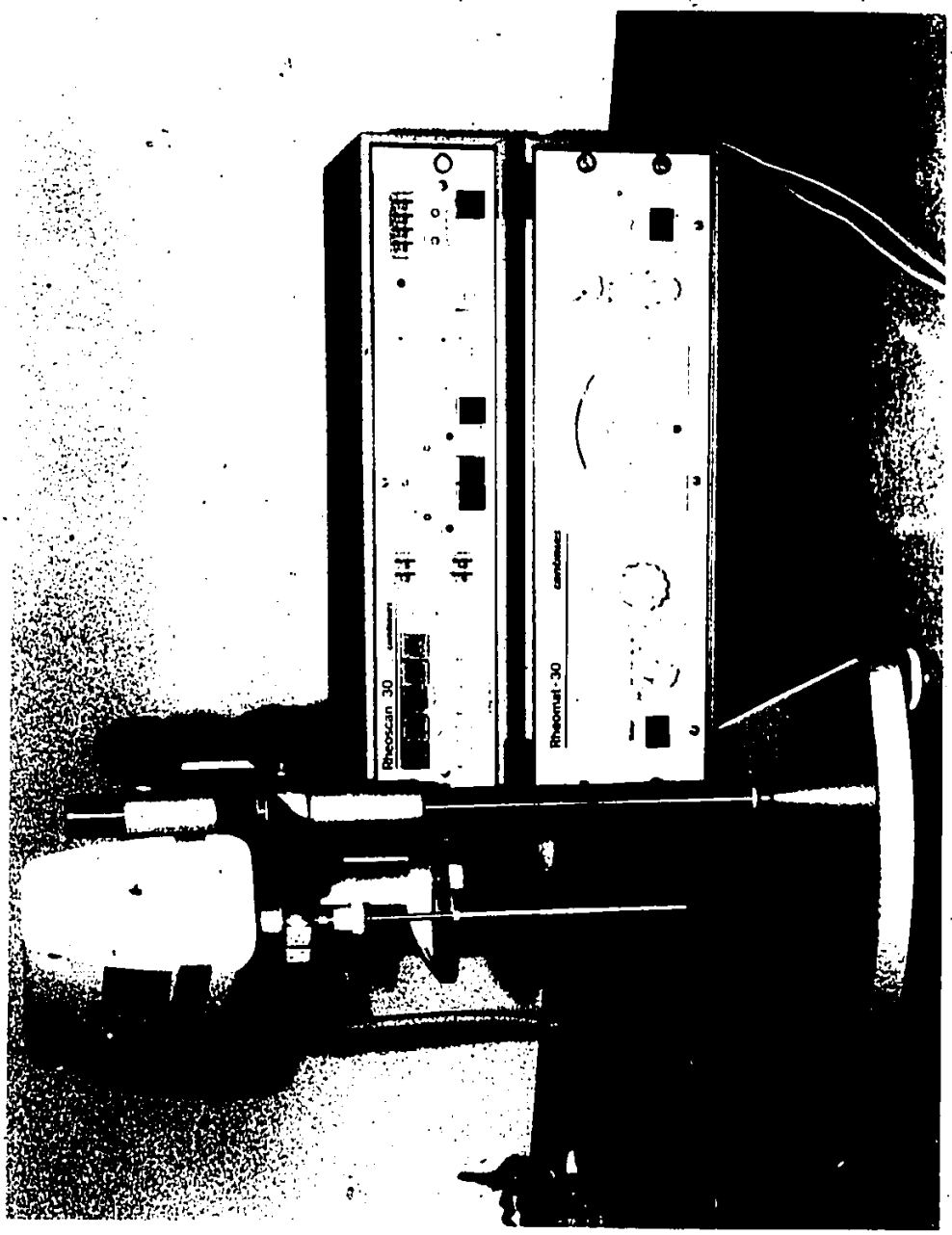

Figure 4.3 Rotary Viscometer

Figure 4.4 Laminar-Turbulent Jet

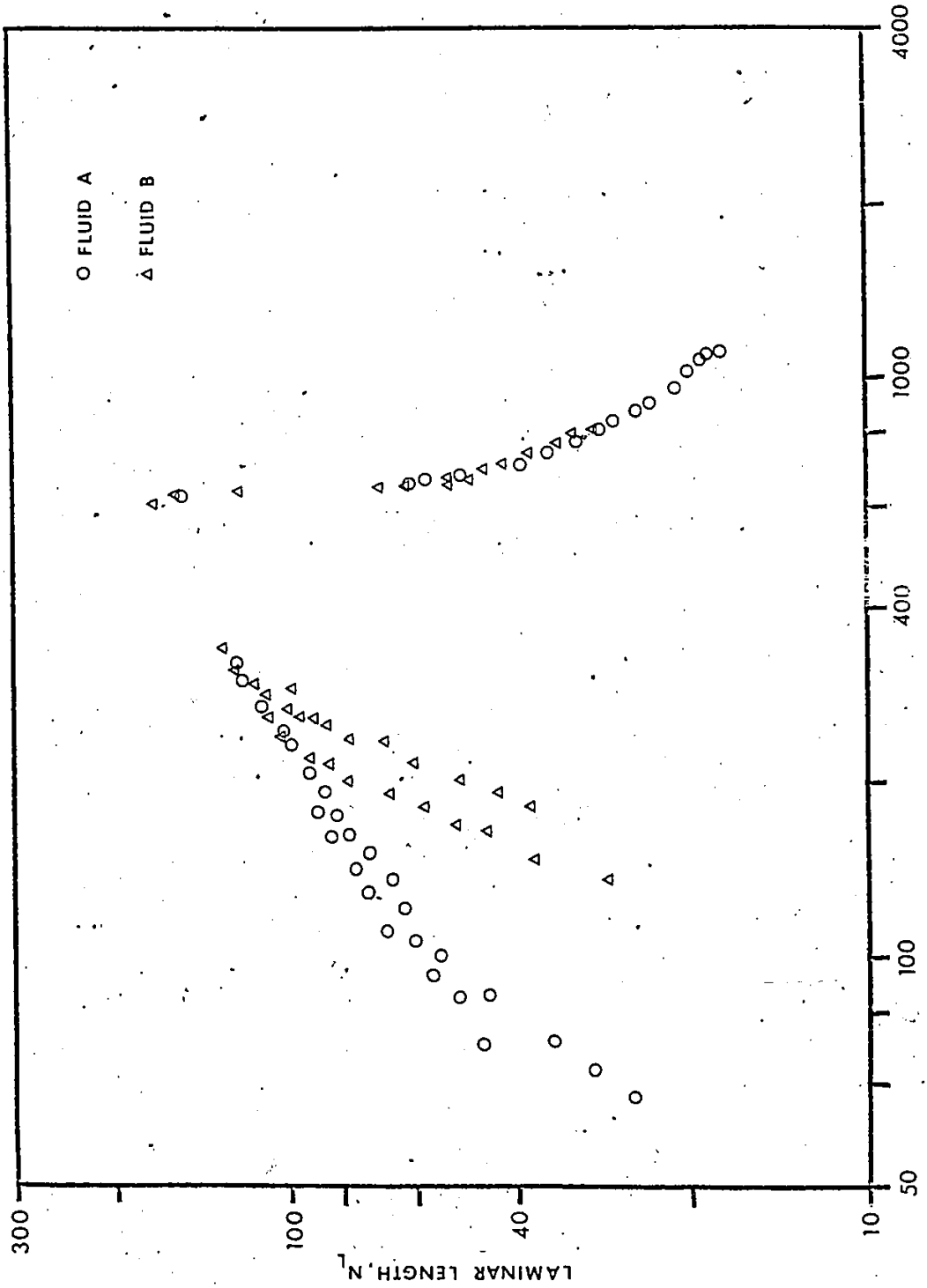

FIGURE 5.1 LAMINAR LENGTH VARIATON WITH REYNOLDS NUMBER

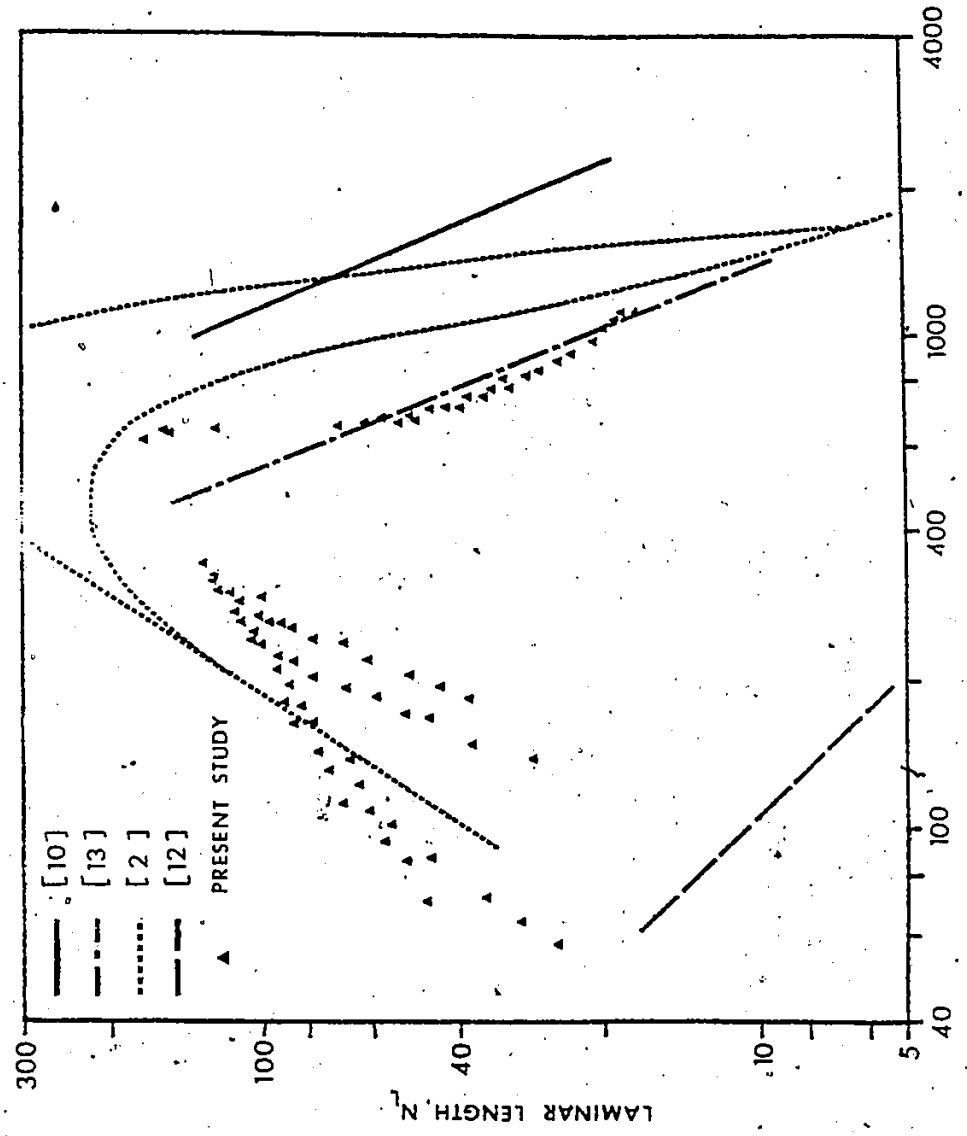

FIGURE 5.2 LAMINAR LENGTH VARIATION WITH REYNOLDS NUMBER (COMPARISON WITH NEWTONIAN STUDIES)

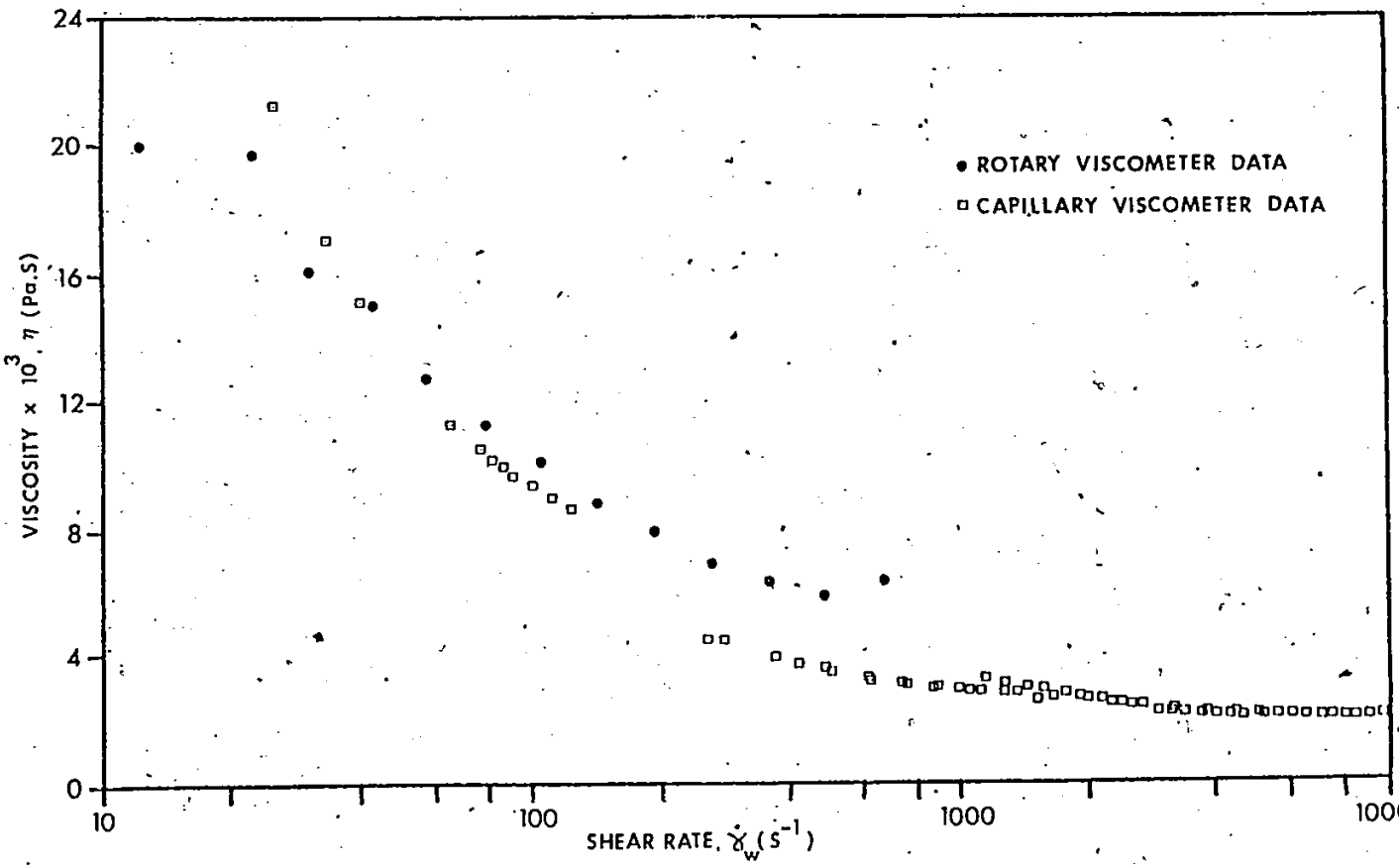

FIGURE 5.3 VISCOSITY DIAGRAM FOR FLUID 'A'

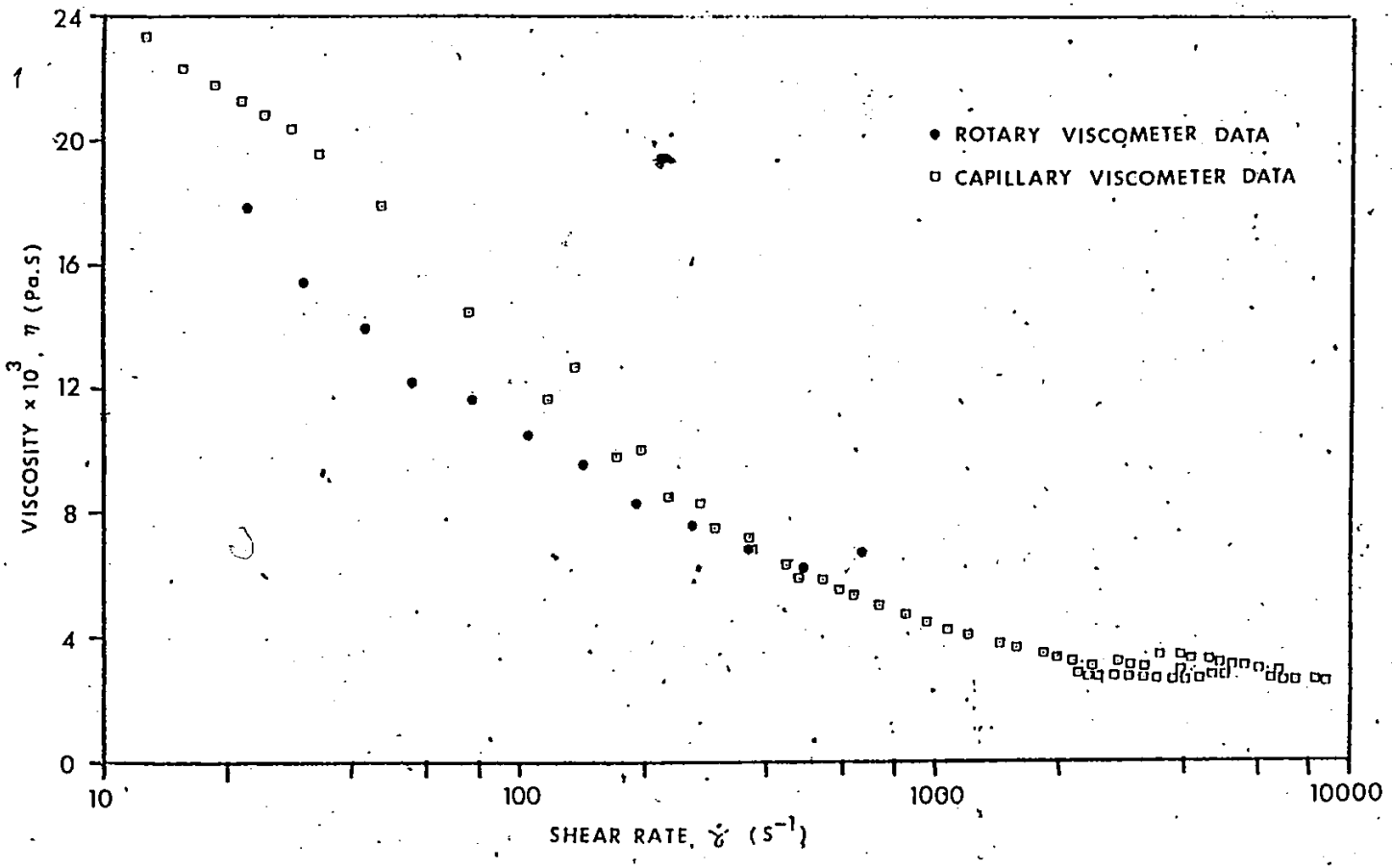

FIGURE 5.4 VISCOSITY DIAGRAM 'FOR FLUID "B'

Table 1

Properties of the Fluids

Fluid	Concentration %	Density Kg/m^3	Flow behaviour index
A	1.207	1000	0.60
B	1.135	998	0.67

Table 2

Rotary Viscometer Data

Fluid = A

Average Temperature = 24.2°C

Shear rate sec^{-1}	Shear Stress Pa	Viscosity x 10^3 Pa sec
12.3	0.246	20.0
22.7	0.448	19.7
30.7	0.493	16.0
41.7	0.627	15.0
56.7	0.717	12.6
77.1	0.873	11.3
104.9	1.052	10.0
142.5	1.245	8.7
193.8	1.523	7.8
263.0	1.814	6.9
358.0	2.217	6.2
487.0	2.844	5.8
662.0	4.209	6.4

Table 3

Rotary Viscometer Data

Fluid = B

Average Temperature = 23.1°C

Shear rate sec^{-1}	Shear Stress Pa	Viscosity x 10^3 Pa sec
22.7	0.403	17.7
30.7	0.470	15.3
41.7	0.582	13.9
56.7	0.694	12.2
77.1	0.896	11.6
104.9	1.097	10.4
142.5	1.366	9.5
193.8	1.612	8.3
263.0	1.993	7.5
358.0	2.441	6.8
487.0	3.045	6.2
662.0	4.422	6.6

Table 4 - Table 16

Capillary Viscometer Data

Table 4

Initial head difference = 2.032 m

Fluid = A

Fitted Curve: $h = A \exp(Bt^2+Ct)$

$\varepsilon = 1.3 \times 10^{-4}$ m^2

where

$A = 2.03135$

$B = -1.34144 \times 10^{-9}$

$C = -1.57114 \times 10^{-4}$

Average Temperature = 20.0°C

Head difference m	Time sec	Shear rate sec^{-1}	Shear Stress Pa	Viscosity$\times 10^3$ Pa sec
2.011	60.6	9970	23.00	2.31
1.991	125.1	9881	22.77	2.30
1.971	190.3	9791	22.54	2.30
1.950	256.3	9701	22.31	2.30
1.930	322.9	9611	22.07	2.30
1.910	390.2	9521	21.84	2.29
1.889	458.3	9430	21.60	2.29
1.869	526.8	9340	21.37	2.29
1.849	595.8	9250	21.14	2.29
1.828	665.9	9159	20.90	2.28
1.808	735.9	9069	20.67	2.28
1.788	807.1	8978	20.44	2.28
1.767	879.2	8887	20.21	2.27
1.747	941.8	8796	19.97	2.27
1.727	1025.4	8704	19.74	2.27
1.706	1099.8	8612	19.51	2.26
1.585	1174.9	8521	19.27	2.26
1.666	1250.6	8429	19.04	2.26
1.645	1327.5	8337	18.81	2.26
1.625	1405.2	8245	18.57	2.25
1.605	1438.4	8206	18.48	2.25
1.584	1563.1	8060	18.11	2.25
1.564	1643.2	7967	17.87	2.24
1.544	1730.0	7868	17.63	2.24

Table 5

Initial head difference = 1.498 m

Fluid = A

Fitted Curve: $h = A \exp(Bt^2+Ct)$

$\varepsilon = 7.0 \times 10^{-7}$ m^2

where

$A = 1.49859$

$B = -4.20527 \times 10^{-11}$

$C = -1.60001 \times 10^{-4}$

Average Temperature - 24.3°C

Head difference m	Time sec	Shear rate sec^{-1}	Shear Stress Pa	Viscosity$\times 10^3$ Pa sec
1.498	0.0	7758	17.13	2.21
1.457	171.7	7549	16.67	2.21
1.437	259.1	7444	16.44	2.21
1.417	348.2	7339	16.20	2.21
1.397	438.4	7234	15.97	2.21
1.376	530.5	7129	15.74	2.21
1.356	622.9	7024	15.51	2.21
1.336	717.4	6919	15.27	2.21
1.315	813.4	6814	15.04	2.21
1.295	910.8	6709	14.81	2.21
1.275	1011.8	6602	14.57	2.21
1.254	1107.1	6502	14.35	2.21
1.234	1211.3	6395	14.11	2.21
1.214	1315.0	6290	13.88	2.21
1.193	1420.7	6185	13.65	2.21
1.173	1527.8	6080	13.42	2.21
1.153	1636.7	5975	13.18	2.21
1.112	1861.1	5765	12.72	2.21
1.092	1976.1	5660	12.49	2.21
1.071	2094.0	5554	12.25	2.21
1.051	2212.7	5450	12.02	2.21
1.031	2332.7	5347	11.79	2.21
1.010	2460.0	5239	11.56	2.21

Table 6

Initial head difference = 1.016 m Fluid = A

Fitted Curve: $h = A \exp(Bt^2+Ct)$ $\varepsilon = 5.7 \times 10^{-7}\ m^2$

where

$A = 1.01559$

$B = 8.37716 \times 10^{-10}$

$C = -1.61601 \times 10^{4}$

Average Temperature = 24.6°C

Head difference m	Time sec	Shear rate sec^{-1}	Shear Stress Pa	Viscosityx10^3 Pa sec
1.016	0.0	5400	11.61	2.15
0.995	122.1	5288	11.38	2.15
0.975	249.4	5174	11.15	2.16
0.955	380.1	5059	10.92	2.16
0.934	513.8	4945	10.69	2.16
0.914	650.9	4830	10.46	2.16
0.894	791.0	4716	10.22	2.17
0.873	936.5	4601	9.99	2.17
0.853	1082.5	4488	9.76	2.17
0.833	1233.7	4374	9.52	2.18
0.814	1388.7	4261	9.29	2.18
0.792	1547.9	4148	9.06	2.18
0.772	1710.9	4035	8.83	2.19
0.541	1879.6	3921	8.59	2.19
0.731	2052.1	3809	8.36	2.20
0.711	2229.6	3697	8.13	2.20
0.690	2414.1	3584	7.90	2.20
0.670	2604.1	3472	7.67	2.21
0.650	2798.6	3361	7.44	2.21
0.629	3003.1	3248	7.20	2.22
0.609	3213.3	3136	6.97	2.22
0.589	3432.3	3024	6.73	2.23
0.568	3650.4	2916	6.51	2.23

Table 7

Initial head difference = 0.863 m Fluid = A

Fitted Curve: $h = A \exp(Bt^2+Ct)$ $\varepsilon = 3.1 \times 10^{-5}\ m^2$

where

$A = 0.86710$

$B = 3.64041 \times 10^{-9}$

$C = -1.48422 \times 10^{-4}$

Average Temperature = 24.5°C

Head difference m	Time sec	Shear rate sec^{-1}	Shear Stress Pa	Viscosity$\times 10^3$ Pa sec
0.863	0.0	4512	9.91	2.20
0.843	188.9	4353	9.64	2.21
0.822	359.2	4216	9.40	2.23
0.802	530.8	4082	9.17	2.24
0.782	710.0	3948	8.94	2.26
0.762	895.6	3815	8.70	2.28
0.741	1089.0	3681	8.47	2.30
0.721	1290.7	3548	8.24	2.32
0.701	1495.7	3418	8.00	2.34
0.680	1712.0	3287	7.77	2.36
0.660	1936.8	3157	7.54	2.39
0.640	2171.8	3028	7.30	2.41
0.619	2417.5	2899	7.07	2.44
0.599	2646.2	2786	6.87	2.46
0.579	2915.6	2658	6.63	2.49
0.558	3200.3	2531	6.40	2.53
0.538	3497.0	2406	6.17	2.56
0.518	3814.0	2281	5.93	2.60
0.497	4151.2	2157	5.70	2.64
0.477	4512.7	2032	5.46	2.69
0.457	4897.3	1909	5.23	2.74
0.436	5308.4	1788	5.00	2.79
0.416	5758.1	1665	4.76	2.86
0.396	6234.3	1547	4.53	2.92
0.375	6704.3	1441	4.32	2.99
0.353	7417.6	1297	4.03	3.11
0.327	8260.1	1150	3.73	3.24

Table 8

Initial head difference = 0.558 m

Fluid = A

Fitted Curve: $h = \exp(Bt^2+Ct)$

$\varepsilon = 6.5 \times 10^{-7}\ m^2$

where

$A = 0.55881$

$B = 2.43372 \times 10^{-9}$

$C = -1.39378 \times 10^{-4}$

Average Temperature = 24.3°C

Head difference m	Time sec	Shear rate sec^{-1}	Shear Stress Pa	Viscosity$\times 10^3$ Pa sec
0.558	0.0	2680	6.39	2.38
0.533	336.9	2531	6.10	2.41
0.508	689.4	2385	5.81	2.44
0.482	1070.2	2239	5.52	2.46
0.457	1478.3	2093	5.23	2.50
0.431	1914.5	1949	4.94	2.53
0.406	2393.6	1804	4.64	2.57
0.381	2893.8	1665	4.36	2.61
0.355	3450.4	1526	4.07	2.66
0.330	4059.7	1388	3.78	2.72
0.304	4740.8	1251	3.49	2.78
0.279	5503.1	1116	3.19	2.86
0.254	6367.8	983	2.90	2.95
0.228	7355.8	853	2.61	3.06
0.203	8517.1	726	2.33	3.20
0.177	9922.1	602	2.04	3.38
0.155	11494.1	492	1.78	3.60

Table 9

Initial head difference = 0.355 m

Fluid = A

Fitted Curve: $h = \exp(A_0+A_1t+A_2t^2 + \ldots +A_7t^8)$

$\varepsilon = 8.4 \times 10^{-10}\ m^2$

where

$A_0 = 2.63922$

$A_1 = -1.24664 \times 10^{-4}$

$A_2 = 1.94258 \times 10^{-9}$

$A_3 = -1.06999 \times 10^{-13}$

$A_4 = 1.05294 \times 10^{-16}$

$A_5 = -2.54026 \times 10^{-20}$

$A_6 = 2.82661 \times 10^{-24}$

$A_7 = -1.51072 \times 10^{-28}$

$A_8 = 3.11649 \times 10^{-33}$

Average Temperature = 25.2°C

Head difference m	Time sec	Shear rate sec^{-1}	Shear Stress Pa	Viscoscityx10^3 Pa sec
0.355	0.0	1525	4.07	2.67
0.330	604.8	1392	3.77	2.71
0.304	1260.8	1269	3.49	2.75
0.279	1997.9	1145	3.19	2.79
0.254	2830.0	1016	2.90	2.86
0.228	3800.8	880	2.61	2.97
0.203	4914.6	746	2.32	3.11
0.117	6265.5	619	2.03	3.28
0.152	7942.5	500	1.74	3.48
0.136	9278.3	420	1.56	3.70
0.127	10130.2	370	1.45	3.92
0.111	11800.0	283	1.28	4.51
0.101	13121.7	260	1.16	4.46

Table 10

Initial head difference = 0.092 m Fluid = A

Fitted Curve: $h = \exp(A_o + A_1 t - A_2 t^2 + A_3 t^3 + A_4 t^4)$ $\varepsilon = 1.2 \times 10^{-7}$ m^2

where

$A_o = 1.29299$

$A_1 = -3.40582 \times 10^{-5}$

$A_2 = 4.64565 \times 10^{-10}$

$A_3 = -9.00045 \times 10^{-16}$

$A_4 = 06.79748 \times 10^{-20}$

Average Temperature = 22.8°C

Head difference m	Time sec	Shear rate sec^{-1}	Shear Stress Pa	Viscosityx10^3 Pa sec
0.092	0.0	122	1.06	8.64
0.087	1556.3	112	1.00	8.90
0.085	2438.5	107	0.97	9.06
0.038	3878.9	100	0.93	9.33
0.080	4437.0	97	0.92	9.43
0.077	5556.5	91	0.89	9.66
0.074	6824.5	86	0.86	9.92
0.072	8029.0	81	0.83	10.11
0.069	9480.5	75	0.80	10.52
0.064	12559.7	65	0.74	11.32
0.052	22448.6	39	0.61	15.18
0.050	25349.0	33	0.58	17.06
0.048	29652.1	25	0.54	21.04

Table 11

Initial head difference = 2.031 m Fluid = B

Fitted Curve: $h = A \exp(Bt^2+Ct)$ $\varepsilon = 9.5 \times 10^{-6}$

where

$A = 2.03119$

$B = 8.76971 \times 10^{-10}$

$C = -1.30860 \times 10^{-4}$

Average Temperature = 22.4°C

Head difference m	Time sec	Shear rate sec^{-1}	Shear Stress Pa	Viscosity$\times 10^3$ Pa sec
2.031	0.0	8828	23.22	2.63
2.006	92.8	8711	22.94	2.63
1.981	190.4	8590	22.65	2.64
1.955	288.5	8470	22.36	2.64
1.930	389.6	8348	22.07	2.64
1.905	490.2	8229	21.78	2.65
1.879	595.0	8107	21.49	2.65
1.854	698.1	7989	21.20	2.65
1.828	807.3	7865	20.91	2.66
1.803	911.4	7750	20.63	2.66
1.778	1026.5	7624	20.32	2.67
1.752	1133.0	7510	20.05	2.67
1.727	1252.7	7384	19.74	2.67
1.701	1361.2	7271	19.47	2.68
1.676	1486.9	7143	19.15	2.68
1.651	1598.0	7032	18.88	2.69
1.625	1727.7	6905	18.57	2.69
1.600	1842.6	6794	18.30	2.69
1.574	1977.8	6666	17.99	2.70
1.54	2096.4	6556	17.72	2.70
1.524	2226.5	6437	17.43	2.71
1.498	2359.7	6319	17.14	2.71
1.473	2494.7	6200	16.85	2.72

Table 12

Initial head difference = 1.752 m

Fitted Curve: $h = A \exp(Bt^2+Ct)$

where

$A = 1.75255$

$B = 2.62776 \times 10^{-9}$

$C = -1.07801 \times 10^{-4}$

Fluid = B

$\varepsilon = 3.8 \times 10^{-6}\ m^2$

Average Temperature = 23.3°C

Head difference m	Time sec	Shear rate sec^{-1}	Shear Stress Pa	Viscosity$\times 10^3$ Pa sec
1.752	0.0	6819	20.04	2.94
1.727	133.3	6676	19.75	2.96
1.701	273.4	6542	19.46	2.97
1.676	417.2	6408	19.17	2.99
1.651	564.0	6275	18.88	3.01
1.625	714.3	6142	18.59	3.03
1.600	865.2	6010	18.29	3.04
1.574	1025.0	5877	18.00	3.06
1.549	1183.4	5746	17.71	3.08
1.542	1328.7	5619	17.42	3.10
1.498	1494.5	5488	17.13	3.12
1.473	1669.2	5357	16.84	3.14
1.447	1845.2	5227	16.55	3.17
1.422	2028.2	5097	16.26	3.19
1.397	2227.9	4965	15.97	3.22
1.371	2420.0	4837	15.68	3.24
1.346	2648.0	4703	15.39	3.27
1.320	2820.3	4581	15.10	3.30
1.295	3026.9	4454	14.81	3.32
1.270	3243.0	4328	14.52	3.35
1.244	3463.2	4202	14.23	3.39
1.219	3703.2	4075	13.94	3.42
1.193	3927.8	3952	13.65	3.45

Table 13

Initial head difference = 1.244 m

Fluid = B

Fitted Curve: $h = A \exp(Bt^2+Ct)$

$\varepsilon = 1.9 \times 10^{-6}\ m^2$

where

$A = 1.11673$

$B = 9.34902 \times 10^{-10}$

$C = -1.31374 \times 10^{-4}$

Average Temperature = 23.3°C

Head difference m	Time sec	Shear rate sec^{-1}	Shear Stress Pa	Viscosity$\times 10^3$ Pa sec
1.244	0.0	5060	14.23	2.81
1.219	169.6	4935	13.94	2.82
1.193	348.2	4810	13.65	2.84
1.168	532.2	4685	13.36	2.85
1.143	721.0	4560	13.07	2.87
1.117	916.2	4435	12.70	2.88
1.092	1115.0	4312	12.49	2.90
1.068	1322.8	4188	12.20	2.91
1.041	1535.6	4065	11.91	2.93
1.016	1757.6	3942	11.62	2.95
0.990	1984.4	3820	11.33	2.97
0.965	2220.5	3698	11.04	2.99
0.939	2463.3	3577	10.74	3.00
0.914	2715.5	3456	10.45	3.02
0.889	2974.6	3336	10.16	3.07
0.838	3524.7	3097	9.58	3.09
0.812	3816.8	2978	9.29	3.12
0.787	4119.9	2860	9.00	3.15
0.762	4437.8	2743	8.71	3.18
0.736	4767.4	2626	8.42	3.21
0.711	5115.8	2510	8.13	3.24
0.685	5480.0	2395	7.84	3.27

Table 14

Initial head difference = 1.117 m

Fluid = B

Fitted Curve: $h = A \exp(Bt^2+Ct)$

$\varepsilon = 2.5 \times 10^{-5}\ m^2$

where

$A = 1.11704$

$B = 1.17268 \times 10^{-9}$

$C = -1.17268 \times 10^{-4}$

Average Temperature = 23.8°C

Head difference m	Time sec	Shear rate sec^{-1}	Shear Stress Pa	Viscosity x 10^3 Pa sec
1.117	0.0	4477	12.77	2.85
1.092	189.5	4360	12.49	2.86
1.066	391.5	4238	12.20	2.88
1.041	599.3	4117	11.91	2.89
1.016	812.5	3997	11.62	2.91
0.990	1031.5	3878	11.33	2.92
0.965	1261.5	3757	11.04	2.94
0.939	1546.3	3614	10.69	2.96
0.914	1741.8	3518	10.46	2.97
0.889	1995.7	3399	10.17	2.99
0.863	2256.1	3282	9.88	3.01
0.838	2529.0	3163	9.59	3.03
0.812	2812.4	3046	9.29	3.05
0.787	3105.5	2929	9.00	3.07
0.762	3416.7	2811	8.71	3.10
0.736	3737.2	2699	8.43	3.12
0.711	4066.5	2582	8.13	3.15
0.685	4410.0	2469	7.84	3.18
0.660	4776.6	2355	7.55	3.21
0.635	5161.2	2242	7.26	3.24
0.609	5565.5	2130	6.97	3.27
0.584	5998.0	2017	6.68	3.31
0.558	6456.0	1905	6.38	3.35

Table 15

Initial head difference = 0.660 m Fluid = B

Fitted Curve: $h = \exp(A_0+A_1t+A_2t^2+\ldots+A_{10}t^{10})$ $\varepsilon = 1.9 \times 10^{-6}$ m^2

where

$A_0 = 1.01324$ $A_5 = 0.15064$

$A_1 = -0.79134$ $A_6 = 1.93511 \times 10^{-2}$

$A_2 = 0.14884$ $A_7 = -0.22477$

$A_3 = -0.28721$ $A_8 = -0.07506$

$A_4 = 0.34025$ $A_9 = -0.40669$

$A_{10} = 0.34922$

Average Temperature = 23.0°C

Head difference m	Time sec	Shear rate sec^{-1}	Shear Stress Pa	Viscosityx10^3 Pa sec
0.660	0.0	2414	7.53	3.12
0.635	39.3	2289	7.28	3.18
0.609	87.8	2145	6.98	3.25
0.584	140.5	2002	6.69	3.34
0.558	196.5	1863	6.39	3.43
0.533	257.6	1726	6.10	3.53
0.508	323.2	1593	5.80	3.64
0.482	395.5	1461	5.51	3.77
0.457	473.2	1335	5.22	3.91
0.431	559.4	1212	4.93	4.07
0.406	655.2	1092	4.64	4.25
0.381	763.0	975	4.35	4.46
0.355	884.4	863	4.07	4.71
0.330	1026.0	753	3.77	5.01
0.304	1189.8	648	3.49	5.38
0.279	1384.4	548	3.20	5.84
0.254	1622.8	452	2.91	6.43
0.228	1925.7	361	2.61	7.24
0.203	2316.8	277	2.32	8.36
0.177	2848.2	202	2.03	10.05
0.152	3606.4	137	1.74	12.71

Table 16

Initial head difference = 0.301 m Fluid = B

Fitted Curve: $h = \exp(A_o + A_1 t + A_2 t^2 + \ldots A_{10} t^{10})$ $\varepsilon = 6.1 \times 10^{-8}$ m^2

where

$A_o = -0.42056$
$A_1 = -1.87582$
$A_2 = -0.15070$
$A_3 = -2.62932$
$A_4 = -3.39313$
$A_5 = -0.57199$
$A_6 = 1.41837$
$A_7 = 3.64316 \times 10^{-2}$
$A_8 = 0.28332$
$A_9 = 1.84961$
$A_{10} = 1.54176$

Average Temperature = 22.4°C

Head difference m	Time sec	Shear rate sec^{-1}	Shear Stress Pa	Viscosityx10^3 Pa sec
.301	0.0	617	3.43	5.56
.275	175.1	537	3.16	5.88
.250	402.1	453	2.87	6.32
.225	672.6	374	2.57	6.87
.199	1002.9	301	2.28	7.56
.194	1423.6	234	1.99	8.51
.148	1982.0	173	1.70	9.83
.123	2762.1	119	1.41	11.78
.098	3888.8	76	1.12	14.57
.072	5588.0	46	.84	17.98
.060	6855.7	34	.69	19.64
.052	7752.8	29	.60	20.44
.047	8455.2	25	.54	20.92
.042	9257.8	22	.48	21.38
.037	10147.5	19	.43	21.85
.032	11233.9	16	.37	22.46
.027	12616.6	13	.31	23.45

Table 17 - Table 24

Nondimensional Laminar Length Data

Table 17

Initial head difference = 2.032 m Fluid = A

Laminar length	Reynolds number
17.8	1116
18.7	1105
19.3	1083
19.6	1065
20.1	1035
20.4	1024
21.0	1008
21.2	995
21.4	997
21.5	961
22.2	945
22.4	934
23.5	913
23.8	903
24.2	894
25:0	882

Table 18

Initial head difference = 1.498 m

Fluid = A

Laminar length	Reynolds number
25.6	876
26.8	862
27.2	850
27.6	834
28.3	819
28.7	803
30.9	793
31.2	785
32.0	778
32.5	768
33.9	755
35.3	745
36.2	734
38.6	718
39.6	708
40.6	701
50	683
57	673
61	662
152	631

Table 19

Initial head difference = 0.863 m

Fluid = A

Laminar length	Reynolds number
123	321
120	295
112	271
108	259
103	246
100	235
93	208
86.8	193
83.1	176
79.8	164
72.5	150
66.5	137
63.2	122
60.6	107
57.0	93
51.8	85
46.7	71

Table 20

Initial head difference = 0.558 m Fluid = A

Laminar length	Reynolds number
100	238
94	209
90.0	177
85.5	160
77.7	143
73.8	128
67.9	111
55.6	101
44.9	87
35.0	71
29.2	64
25.4	57

Table 21

Initial head difference = 2.031 m Fluid = B

Laminar length	Reynolds number
29.1	815
31.6	809
32.0	801
32.4	790
32.9	778
34.0	771
35.7	761
36.9	749
38.3	740
39.9	730
42.2	717
42.4	708
45	698
47	690
52	672
36 to 60	667
38 to 77	660
42 to 80	654
44 to 96	648
52 to 192	640
58 to 254	638
68 to 254	632
80 to 254	623
89 to 254	606

Table 22

Initial head difference = 1.752 m Fluid = B

Laminar length	Reynolds number
122	313
119	301
99	283
90	263
75	254
68	240

Table 23

Initial head difference = 1.244 m Fluid = B

Laminar length	Reynolds number
128	317
124	306
117	205
109	282
100	272
94	260
86	249
79	238
68	226
60	215
50	204
43.4	193
37.2	182

Table 24

Initial head difference = 1.117 m Fluid = B

Laminar length	Reynolds number
129	339
122	315
114	293
111	273
108	259
103	239
92	224
85	215
78	201
66.8	192
57.5	181
51.0	171
45.5	166
37.6	148
27.8	137

APPENDIX A

Preparation of Milling Yellow Solution

Milling Yellow is available in powdered form. The dye powder is bright yellow in colour and has a low density. It can be obtained from Keystone Aniline and Chemicals Co., Chicago, Illinois, U.S.A. The dye used in the present study was Keyacid Milling Yellow 3NGS code 801-044-51-5, Lot B2109. The procedure for preparing the solution is given below.

(a) Distilled water was brought to boiling state as the dye powder does not dissolve in water at room temperature.

(b) Dye powder in the amount that yielded a solution of 1% by weight was then added to the boiling water in small batches. This is the maximum concentration that can be prepared initially. To obtain solutions of higher concentration, the 1% solution must be heated to evaporate the excess water.

(c) Each time the dye powder was added the solution was stirred continuously to dissolve it completely.

(d) The solution was then allowed to cool down to room temperature.

(e) The pH value of the solution has to be approximately 7 in order to obtain a fluid which has good birefringent characteristics. For this purpose, a small amount of phosphoric acid (40% concentration) was added to the solution. Instead of measuring the pH value, in the present work, the solution was placed between the polarizer and analyzer and stirred continuously in order to produce motion. Acid was added until satisfactory clarity and birefringent characteristic (fringes)

were achieved.

(f) The solution was heated to increase the concentration to values above 1%, when required.

(g) The solution was then stored in plastic container.

In the present study, solutions having concentrations of 1.204% and 1.135% were used.

Major factors which influence the birefringent characteristics of the fluid are its concentration, acidity and age. Prolonged storage of a solution improves its birefringence. Solutions having a concentration of 1% by weight and greater are quite birefringent. A higher concentration, however, yields a more viscous solution. Solutions having concentration in the range of 1.2% to 1.6% have ideal properties.

APPENDIX B

Viscosity Determination using Non-Linear Parameter Estimation Technique and "Falling Head" Capillary Viscometer

One of the most common instruments used to determine the rheological properties of a Non-Newtonian fluid is a capillary viscometer. The experimental set up used for measuring the laminar length in the present study also serves as a capillary viscometer. In a capillary viscometer the flow rate of the fluid and the corresponding frictional pressure drop are measured. This is accomplished by measuring the drop in head and the corresponding interval of time. From the relationship between the head and time, the viscosity of the fluid at various shear rates can be deduced. In order to establish the relationship between the head and time, a curve fitting technique based on the least square method is employed.

Before discussing the above mentioned parameter estimation technique, it is necessary to develop the relationship used to determine the viscosity of the fluid. This formulation is already presented in references [8] and [20]. However, for the sake of completeness it is given here.

Fluid from the upstream tank flows into the downstream tank due to the head difference. Let h_i be the difference in levels of the fluid in the upstream and downstream tank at time t. If Δh is the drop in the liquid level in one of the tanks during the time interval Δt, the head difference at time $t + \Delta t$ is given by $h = h_i - 2(\Delta h)$.

The flow rate can be written as

$$Q = A_T \frac{\Delta h}{\Delta t} . \qquad \ldots(B.1)$$

where A_T is the area of the upstream tank. Neglecting minor losses, we can write the pressure drop as

$$\Delta p = \rho g h \qquad \ldots(B.2)$$

For steady, fully developed flow of a Non-Newtonian, time independent fluid through a vertical capillary tube (Ref. [19]) the wall shear stress is

$$\tau_\omega = \frac{R\,\Delta p}{2\ell} = \frac{R\,\rho g h}{2\ell} \qquad \ldots(B.3)$$

and the shear rate.

$$\dot{\gamma} = f(\tau) \qquad \ldots(B.4)$$

It can be shown that

$$\frac{Q}{\pi R^3} = \frac{1}{\tau_\omega^3} \int_0^{\tau_\omega} \tau^2 f(\tau)\, d\tau \qquad \ldots(B.5)$$

and the apparent fluidity is

$$\phi_e = \frac{1}{\eta} = \frac{8LQ}{\pi R^4} \frac{1}{\Delta p} \qquad \ldots(B.6)$$

Substituting equations (B.1) and (B.2) into (B.6) we obtain

$$\ell n\, h = \left(-\frac{2\pi R^4 \rho g}{8\ell A_T}\, \phi_e\right) t + c \qquad \ldots(B.7)$$

Using (B.3) and substituting for Δp in (B.6) yields

$$\phi_e = \frac{4Q}{\pi R^3 \tau_\omega} = \frac{4}{\tau_\omega^4} \int_0^{\tau_\omega} \tau^2 f(\tau)\, d\tau \qquad \ldots(B.8)$$

When the above equation is differentiated with respect to τ_ω using Leibnitz's rule we get

$$\frac{d\phi_e}{d\tau_\omega} = -4\left[\frac{\phi_e}{\tau_\omega} - \frac{f(\tau_\omega)}{\tau_\omega^2}\right] \qquad \ldots(B.9)$$

Rearranging this we obtain

$$\frac{\gamma_\omega}{\tau_\omega} = -\phi_e\left[1 + \frac{1}{4}\frac{d\ \ell n\ \phi_e}{d\ \ell n\ \tau_\omega}\right] \qquad \ldots(B.10)$$

Defining $S = \frac{2\pi R^4 g}{8\ell A_T}$ and $m = -S\rho\phi_e$ and by making use of equation (B.3) we can write equation (B.10) as

$$\frac{\gamma_\omega}{\tau_\omega} = -\frac{m}{S\rho}\left[1 + \frac{1}{4m^2}\frac{dm}{dt}\right] \qquad \ldots(B.11)$$

From equation (B.7) we see that

$$m = \frac{d(\ell nh)}{dt} \qquad \ldots(B.12)$$

In order to find out the viscosity of the fluid at a particular shear rate, we need to know the values of m and $\frac{dm}{dt}$ at that shear rate.

This is evident from equation (B.11). In other words, once the relationship between h and t is known the viscosity determination is simple. A curve fitting technique was employed to formulate this relationship. Two methods, one in the high shear rate region and the other one in the intermediate and low shear rate regions, were used.

A relationship of the form

$$h = A \exp (Bt^2 + Ct) \qquad \ldots(B.13)$$

was used in the high shear rate region ($\dot{\gamma} \geq 1000$). The parameters A, B and C were obtained using the least-square principle. Those values of A, B and C which gave the minimum sum of the error squared were taken to be the best estimates. This method worked very well in the high shear rate region. In low shear rate region this relationship was not a good approximation to the data.

In the low shear rate region a relationship of the form

$$h = \exp (A_o + A_1 t + A_2 t^2 + \ldots + A_n t^n) \text{ where } n \leq 10 \qquad \ldots(B.14)$$

was used to fit the head-time data. This nth degree polynomial fitting of the $\ln h - t$ data gave better results than the previous second degree polynomial fitting.

Curve fitting of the second order polynomial was carried out using a program written in BASIC and run on an APPLE II PLUS computer. The nth degree polynomial fitting was carried out using a curve fitting package available on the department's IM 70 Minicomputer. A copy of the

BASIC program is given in Appendix C.

Once the parameters were estimated the values of m and $\frac{dm}{dt}$ were obtained as

$$m = \frac{d}{dt} (\ell n\ h) = 2Bt + c \qquad \ldots(B.15)$$

and

$$\frac{dm}{dt} = 2B \qquad \ldots(B.16)$$

for the second degree polynomial. For the nth degree polynomial by using equation (B.13)

$$m = A_1 + 2A_2t + 3A_3t^2 + \ldots + n\ A_n t^{n-1} \qquad \ldots(B.17)$$

and

$$\frac{dm}{dt} = 2A_2 + 6A_3t + 12A_4t^2 + \ldots + n(n-1)\ A_n t^{n-2} \ldots(B.18)$$

were found. In order to obtain viscosity, the values of m, $\frac{dm}{dt}$, S and ρ were substituted into equation (B.11) which was rearranged as follows:

$$\eta = \frac{1}{\left(\frac{\dot{\gamma}_\omega}{\tau_\omega}\right)} = \frac{-S\rho}{m\left[1 + \frac{1}{4m^2}\frac{dm}{dt}\right]} \qquad \ldots(B.19)$$

The shear stress was calculated using equation (B.3) and the shear rate was found using

$$\dot{\gamma}_\omega = \frac{\tau_\omega}{\eta} \qquad \ldots(B.20)$$

The head-time data that was taken during the present study are given in Tables 4 through 16. The values of viscosity, shear rate and shear stress are also included.

APPENDIX C

COMPUTER PROGRAM

```
50 REM M,NIT ARE THE NUMBER OF
   DATA POINTS AND NUMBER OF IT
   ERATIONS TO BE DONE RESPECTI
   VELY
100 M = 23
120 NIT = 30
140 DIM H(M),T(M),CALH(M),A(NIT)
   ,B(NIT)
160 DIM C(NIT),D(NIT),NOP(M),ERS
   Q(NIT),P(10,10)
170 REM A(1),B(1)AND C(1) ARE T
   HE INITIAL ESTIMATES OF THE
   PARAMETERS
180 A(1) = 69
200 B(1) = 1E - 10
220 C(1) = - 1E - 06
260 FOR IT = 1 TO NIT
280 FOR I = 1 TO 4
300 FOR J = 1 TO 5
320 P(I,J) = 0
340 NEXT J
360 NEXT I
380 FOR I = 1 TO M
400 READ T(I)
410 H(I) = 70 - I
420 NOP(I) = EXP (B(IT) * T(I) *
   T(I) + C(IT) * T(I))
440 P(1,1) = P(1,1) + (NOP(I) ^ 2
   )
460 P(1,2) = P(1,2) + A(IT) * ((T
   (I) * NOP(I)) ^ 2)
480 P(1,3) = P(1,3) + A(IT) * T(I
   ) * (NOP(I) ^ 2)
520 P(1,4) = P(1,4) + NOP(I) * (N
   OP(I) * A(IT) - H(I))
540 P(2,1) = P(1,2)
560 P(2,2) = P(2,2) + (A(IT) * NO
   P(I) * (T(I) ^ 2)) ^ 2
580 P(2,3) = P(2,3) + T(I) * ((A(
   IT) * NOP(I) * T(I)) ^ 2)
620 P(2,4) = P(2,4) + ((A(IT) * T
   (I) * NOP(I)) ^ 2) - ((A(IT)
    * NOP(I) * H(I)) * (T(I) ^
   2))
640 P(3,1) = P(1,3)
660 P(3,2) = P(2,3)
680 P(3,3) = P(3,3) + (A(IT) * T(
   I) * NOP(I)) ^ 2
720 P(3,4) = P(3,4) + (T(I) * (A(
   IT) * NOP(I)) ^ 2) - (T(I) *
   A(IT) * NOP(I) * H(I))
740 NEXT I
760 P(1,4) = - P(1,4)
780 P(2,4) = - P(2,4)
800 P(3,4) = - P(3,4)
842 FOR K = 1 TO 3
844 FOR J = 1 TO 4
846 P(K,J) = P(K,J) / 1E03
848 NEXT J
850 NEXT K
1500 N = 3
1520 FOR I = 1 TO N
1540 IF I = 1 GOTO 1800
1560 FOR K = 1 TO I - 1
1580 FOR J = 1 TO N + 1
1600 IF J = I GOTO 1760
1620 A = P(I,J)
1640 B = P(K,I)
1660 C = P(I,I)
1680 D = P(K,J)
1700 E = A * B
1720 F = C * D
1740 P(K,J) = E - F
1760 NEXT J
1780 NEXT K
1800 FOR K = I + 1 TO N
```

```
1820 IF K > N GOTO 2100
1840 FOR J = 1 TO N + 1
1860 IF J = I GOTO 2020
1880 A = P(I,J)
1900 B = P(K,I)
1920 D = P(K,J)
1940 C = P(I,I)
1960 E = A * B
1980 F = C * D
2000 P(K,J) = E - F
2020 NEXT J
2040 P(K,I) = 0
2060 NEXT K
2080 NEXT I
2100 FOR I = 1 TO N
2120 X(I) = P(I,N + 1) / P(I,I)
2262 V = X(1)
2263 U = X(2)
2264 W = X(3)
2280 NEXT I
2300 PRINT U,V,W
2410 A(IT + 1) = V + A(IT)
2420 B(IT + 1) = U + B(IT)
2430 C(IT + 1) = W + C(IT)
2432 PRINT "A";IT + 1;")=";A(IT
   + 1)
2434 PRINT "B";IT + 1;")=";B(IT
   + 1)
2436 PRINT "C";IT + 1;")=";C(IT
   + 1)
2440 ERSQ(IT) = 0
2450 FOR I = 1 TO M
2460 CALH(I) = A(IT + 1) * EXP (
   (B(IT + 1) * T(I) * T(I)) +
   (C(IT + 1) * T(I)))
2470 ERR = CALH(I) - H(I)
2472 PRINT H(I),CALH(I),(ERR / H
   (I)) * 100
2480 ERSQ(IT) = ERSQ(IT) + (ERR ^
   2)
2482 FOR S = 1 TO 50
2483 NEXT S
2490 NEXT I
2495 PRINT "ERSQ(";IT;")=";ERSQ(
   IT)
2500 IF IT = 1 GOTO 2530
2510 IF ERSQ(IT) < ERSQ(IT - 1) GOTO
   2530
2520 IF ERSQ(IT) > ERSQ(IT - 1) GOTO
   2550
2530 RESTORE
2540 NEXT IT
2550 RAD = 0.71045E - 03
2570 NEL = 0.3048
2590 OD = 0.1524
2610 RHO = 1000
2630 CAP = RAD * RHO * 9.810 / (2
   * NEL)
2650 S = (RAD ^ 4) * 9.810 / (NEL
   * OD * OD)
2670 FOR I = 1 TO M
2690 STRESS = CAP * H(I) * 2.54E -
   02
2710 SLP = (2 * B(IT) * T(I)) + C
   (IT)
2730 DER = 2 * B(IT)
2750 U = DER / (4 * SLP * SLP)
2770 V = SLP / (S * RHO)
2790 VIS = - 1 / (V * (1 + U))
2810 SHRTE = STRESS / VIS
2830 PRINT "STRESS=";STRESS,"SH
   RATE=";SHRTE,"VISCO=";VIS
2850 NEXT I
2870 END
3310 DATA
```

APPENDIX D

UNCERTAINTY ANALYSIS

The data used in the following analysis are taken for Fluid B. In this analysis laminar lengths for four different Reynolds number are considered.

N_L = 29, Re = 815 (Table 21)
(L = 41.4 mm)

N_L = 44.4 to 96, Re = 648 (Table 21)
(L = 63 to 136 mm)

N_L = 120, Re = 301 (Table 22)
(L = 170 mm)

N_L = 37.6, Re = 148 (Table 24)
(L = 53.4 mm)

For the uncertainty analysis of viscosity and other related quantities the following data are used.

h = 1.9040 m
t = 490.20 sec
Δh = 0.063 m
(Table 11)

The uncertainty in the following quantities are estimated; d, N_L, h, $\frac{dh}{dt}$, $\dot{m}$, $\frac{dm}{dt}$, A_T, S, ρ, η, τ_ω, $\dot{\gamma}_\omega$, Q, V and Re.

(1) Capillary Diameter (d)

$$d = \left(\frac{4m}{\pi \rho_{Hg} \ell}\right)^{1/2}$$

where $m = (4.62 \pm 0.01) \times 10^{-3}$ kg

$\ell = (225 \pm 5) \times 10^{-3}$ m

$\rho_{Hg} = (13.5 \pm 0.2) \times 10^{3}$ kg/m^3

also

$$W_d = \left[\left(\frac{\partial d}{\partial m} W_m\right)^2 + \left(\frac{\partial d}{\partial \ell} W_\ell\right)^2 + \left(\frac{\partial d}{\partial \rho_{Hg}} W_{\rho_{Hg}}\right)^2 \right]^{1/2}$$

$$= \left[\left(\frac{W_m}{2m}\right)^2 + \left(-\frac{W_\ell}{2\ell}\right)^2 + \left(-\frac{W_{\rho_{Hg}}}{2\rho_{Hg}}\right)^2 \right]^{1/2} \times d$$

which gives $d = (1.42 \pm 0.02) \times 10^{-3}$ m (±1.4%)

(2) Non dimensional Laminar Length (N_L)

The uncertainty introduced in the measurement of laminar length, L, is due to the following:

(a) The diameter of the wire which is used to locate the transition point.

(b) The difficulty in locating the transition point by visual observation.

The laminar length, L, and the corresponding uncertainty, W_L, for different Reynolds number ranges are estimated as follows:

$L = (41.4 \pm 2.5) \times 10^{-3}$m (±6%) for $700 < Re < 1100$

$L = (99 \pm 36) \times 10^{-3}$m (±35%) for $600 < Re < 700$

$L = (170 \pm 20) \times 10^{-3}$m (±12%) for $200 < Re < 350$

$L = (53.4 \pm 5.5) \times 10^{-3}$m (±10%) for $50 < Re < 200$

The non dimensional laminar length is given as

$$N_L = \left(\frac{L}{d}\right)$$

where $d = (1.42 \pm 0.02) \times 10^{-3}$m

and the values of L are as given above.

Also

$$W_{N_L} = \left[\left(\frac{\partial N_L}{\partial L} W_L\right)^2 + \left(\frac{\partial N_L}{\partial d} W_d\right)^2\right]^{1/2} = \left[\left(\frac{W_L}{L}\right)^2 + \left(-\frac{W_d}{d}\right)^2\right]^{1/2} \times N_L$$

which gives

$N_L = 29 \pm 3$ (±10%) for $700 < Re < 1100$

$= 70 \pm 25$ (±37%) for $600 < Re < 700$

$= 120 \pm 14$ (±12%) for $200 < Re < 350$

$= 37.6 \pm 3.9$ (±10%) for $50 < Re < 200$

(3) . Head (h)

The head is calculated using the following equation

$$h = h_i - 2\Delta h$$

where $h_i = (2031 \pm 20) \times 10^{-3}$ m

$\Delta h = (63 \pm 2) \times 10^{-3}$ m

also

$$W_h = \left[\left(\frac{\partial h}{\partial h_i} W_{h_i}\right)^2 + \left(\frac{\partial h}{\partial \Delta h} W_{\Delta h}\right)^2\right]^{1/2}$$

$$= \left[(W_{h_i})^2 + (-2W_{\Delta h})^2\right]^{1/2}$$

which gives $h = (1905 \pm 20) \times 10^{-3}$ m $(\pm 1.1\%)$

(4) Slope of h versus t (dh/dt):

The h versus t data are curve fitted using the relation

$$h = A \exp (Bt^2 + Ct)$$

$$\frac{dh}{dt} = A \exp (Bt^2 + Ct) \cdot (2Bt + C)$$

$$= h (2Bt + C)$$

where $h = (1904 \pm 20) \times 10^{-3}$ m

$B = 8.76971 \times 10^{-10} \pm 0$

$C = -1.30860 \times 10^{-4} \pm 0$

$t = (490.2 \pm 0.5)$ sec

also

$$W_{dh/dt} = \left[\left(\frac{\partial^{(\partial h/\partial t)}}{\partial_h} W_h\right)^2 + \left(\frac{\partial^{(\partial h/\partial t)}}{\partial_t} W_t\right)^2\right]^{1/2}$$

which gives $\frac{dh}{dt} = (-0.248 \pm 0.003) \times 10^{-3} \frac{m}{s}$ $(\pm 1.2\%)$

(5) Slope of (dh/dt) versus t. (d^2h/dt^2):

We have $\frac{dh}{dt} = h(2Bt + C)$

$$\frac{d^2h}{dt^2} = (2Bt + C)\frac{dh}{dt} + 2Bh$$

where $B = 8.76971 \times 10^{-10} \pm 0$

$C = -1.30860 \times 10^{-4} \pm 0$

$t = (490.2 \pm 0.5)$ sec

$h = (1904 \pm 20) \times 10^{-3}$ m

$\frac{dh}{dt} = (-0.248 \pm 0.003) \times 10^{-3}$ m/sec

also

$$W_{d^2h/dt^2} = \left\{ \left[W_h \frac{\partial}{\partial h}\left(\frac{d^2h}{dt^2}\right)\right]^2 + \left[W_{dh/dt} \frac{\partial}{\partial \frac{dh}{dt}}\left(\frac{d^2h}{dt^2}\right)\right]^2 + \left[W_t \frac{\partial}{\partial t}\left(\frac{d^2h}{dt^2}\right)\right]^2 \right\}$$

$$= \left\{ [2B\, W_h]^2 + [(2Bt + C)\, W_{dh/dt}]^2 + \left[2B \frac{dh}{dt}\, W_t\right]^2 \right\}^{1/2}$$

which gives $\frac{d^2h}{dt^2} = (355 \pm 4) \times 10^{-10} \frac{m}{sec^2}$ ($\pm 1.1\%$)

(6) Slope of ℓn h versus t (m)

$$m = \frac{d}{dt}(\ell n\, h)$$

$$= \frac{1}{h}\frac{dh}{dt}$$

where $h = (1904 \pm 20) \times 10^{-3}$ m

$\frac{dh}{dt} = (-0.248 \pm 0.003) \times 10^{-3}$ m/sec

also

$$W_m = \left[\left(\frac{\partial m}{\partial h} W_h\right)^2 + \left(\frac{\partial m}{\partial\, dh/dt}\, W_{dh/dt}\right)^2\right]^{1/2}$$

$$= \left[\left(-\frac{W_h}{h}\right)^2 + \left(\frac{W_{dh/dt}}{dh/dt}\right)^2\right]^{1/2} \times m$$

which gives $m = (-130 \pm 2) \times 10^{-6}$ ℓn of head in metres/sec (±1.5%)

(7) Slope of m versus t (dm/dt)

$$\frac{dm}{dt} = \frac{d}{dt}\left[\frac{1}{h}\frac{dh}{dt}\right]$$

$$= \frac{1}{h}\left[\frac{d^2h}{dt^2} - \frac{1}{h}\left(\frac{dh}{dt}\right)^2\right]$$

where $h = (1904 \pm 20) \times 10^{-3}$ m

$\frac{dh}{dt} = (-0.248 \pm 0.003) \times 10^{-3}$ m/sec

$\frac{d^2h}{dt^2} = (355 \pm 4) \times 10^{-10}$ m/sec^2

also

$$W_{\frac{dm}{dt}} = \left\{\left[W_h \frac{\partial}{\partial h}(dm/dt)\right]^2 + \left[W_{\frac{dh}{dt}} \frac{\partial}{\partial \frac{dh}{dt}}\left(\frac{dm}{dt}\right)\right]^2 + \left[W_{\frac{d^2h}{dt^2}} \frac{\partial}{\partial d^2h/dt^2}\left(\frac{dm}{dt}\right)\right]^2\right\}^{1/2}$$

which gives $\frac{dm}{dt} = (7 \pm 5) \times 10^{-10}$ ℓn of head in metres/sec^2 (±29%)

(8) Area of Tank (A_T)

$$A_T = \frac{\pi D^2}{4}$$

where $D = (152 \pm 3) \times 10^{-3}$ m

also

$$W_{A_T} = 2A_T \frac{W_D}{D}$$

which gives $A_T = (18.2 \pm 0.7) \times 10^{-3}$ m^2 ($\pm 3.9\%$)

(9) Parameter S

$$S = \frac{2\pi R^4 g}{8\ell A_T} = \frac{\pi d^4 g}{64\ell A_T}$$

where $d = (1.42 \pm 0.02) \times 10^{-3}$ m

$\ell = (304 \pm 2) \times 10^{-3}$ m

$A_T = (18.2 \pm 0.7) \times 10^{-3}$ m^2

also

$$W_S = \left[\left(\frac{\partial S}{\partial d} W_d\right)^2 + \left(\frac{\partial S}{\partial A_T} W_{A_T}\right)^2 + \left(\frac{\partial S}{\partial \ell} W_\ell\right)^2\right]^{1/2}$$

$$= Sx\left[\left(\frac{4W_d}{d}\right)^2 + \left(-\frac{W_{A_T}}{A_T}\right)^2 + \left(-\frac{W_\ell}{\ell}\right)^2\right]^{1/2}$$

which gives $S = (3.6 \pm 0.2) \times 10^{-10} \frac{m^2}{sec^2}$ ($\pm 5.6\%$)

(10) Density of Milling Yellow (ρ)

$$\rho = \frac{m}{V}$$

where $m = (29.95 \pm 0.01) \times 10^{-3}$ Kg

$V = (30 \pm 0.5) \times 10^{-6}$ m^3

also

$$W_\rho = [(\frac{\partial \rho}{\partial m} W_m)^2 + (\frac{\partial \rho}{\partial V} W_V)^2]^{1/2}$$

$$= \rho x[(\frac{W_m}{m})^2 + (-\frac{W_V}{V})^2]^{1/2}$$

which gives $\rho = (998 \pm 16) \frac{kg}{m^3}$ (±1.6%)

(11) Apparent Viscosity (η)

$$\eta = -\frac{S\rho}{m}[1 + \frac{1}{4m^2}(\frac{dm}{dt})]^{-1}$$

where $S = (3.6 \pm 0.2) \times 10^{-10}\ m^2/sec^2$

$\rho = (998 \pm 16)\ kg/m^3$

$m = (-130 \pm 2) \times 10^{-6} \frac{\ell n \text{ of head in metres}}{sec}$

$\frac{dm}{dt} = (17 \pm 5) \times 10^{-10} \frac{\ell n \text{ of head in metres}}{sec^2}$

also

$$W_\eta = [(\frac{\partial \eta}{\partial S} W_S)^2 + (\frac{\partial \eta}{\partial \rho} W_\rho)^2 + (\frac{\partial \eta}{\partial m} W_m)^2$$

$$+ (\frac{\partial \eta}{\partial \frac{dm}{dt}} \cdot W_{\frac{dm}{dt}})^2]^{1/2}$$

which gives $\eta = (2.67 \pm 0.17) \times 10^{-3}$ Pa sec (±6.4%)

(12) Wall Shear Stress (τ_ω)

$$\tau_\omega = \frac{R\rho gh}{2\ell} = \frac{\rho ghd}{4\ell}$$

where $d = (1.42 \pm 0.02) \times 10^{-3}$ m

$\rho = (998 \pm 16)$ kg/m^3

$h = (1904 \pm 20) \times 10^{-3}$ m

$\ell = (304 \pm 2) \times 10^{-3}$ m

also

$$W_{\tau_\omega} = \left[\left(\frac{\partial \tau_\omega}{\partial d} W_d\right)^2 + \left(\frac{\partial \tau_\omega}{\partial \ell} W_\ell\right)^2 + \left(\frac{\partial \tau_\omega}{\partial h} W_h\right)^2 + \left(\frac{\partial \tau_\omega}{\partial \rho} W_\rho\right)^2\right]^{1/2}$$

$$= \tau_\omega \times \left[\left(\frac{W_d}{d}\right)^2 + \left(-\frac{W_\ell}{\ell}\right)^2 + \left(\frac{W_h}{h}\right)^2 + \left(\frac{W_\rho}{\rho}\right)^2\right]^{1/2}$$

which gives $\tau_\omega = (21.77 \pm 0.54)$ Pa (±2.5%)

(13) Wall Shear Rate ($\dot{\gamma}_\omega$)

$$\dot{\gamma}_\omega = \tau_\omega / \eta$$

where $\tau_\omega = (21.77 \pm 0.54)$ Pa

$\eta = (2.67 \pm 0.17) \times 10^{-3}$ Pa S

also

$$W_{\dot{\gamma}_\omega} = \left[\left(\frac{\partial \dot{\gamma}_\omega}{\partial \eta} W_\eta\right)^2 + \left(\frac{\partial \dot{\gamma}_\omega}{\partial \tau_\omega} W_{\tau_\omega}\right)^2\right]^{1/2}$$

$$= \dot{\gamma}_\omega \times \left[\left(-\frac{W_\eta}{\eta}\right)^2 + \left(\frac{W_{\tau_\omega}}{\tau_\omega}\right)^2\right]^{1/2}$$

which gives $\dot{\gamma}_\omega = (8.154 \pm 0.555) \times 10^3$ sec^{-1} (±6.8%)

(14) Volumetric Flow Rate (Q)

$$Q = -\frac{A_T}{2}\frac{dh}{dt}$$

where $A_T = (18.2 \pm 0.7) \times 10^{-3}\ m^2$

$$\frac{dh}{dt} = (-0.248 \pm 0.003) \times 10^{-3}\ m/sec$$

also

$$W_Q = \left[\left(\frac{\partial Q}{\partial A_T} W_{A_T}\right)^2 + \left(\frac{\partial Q}{\partial \frac{dh}{dt}} W_{\frac{dh}{dt}}\right)^2\right]^{1/2}$$

$$= Q \times \left[\left(-\frac{W_{A_T}}{A_T}\right)^2 + \left(-\frac{W_{dh/dt}}{dh/dt}\right)^2\right]^{1/2}$$

which gives $Q = (23 \pm 1) \times 10^{-7}\ m^3/sec$ (4.4%)

(15) Average Velocity (V)

$$V = \frac{4Q}{\pi d^2}$$

Where $Q = (23 \pm 1) \times 10^{-7}\ m^3/sec$

$$d = (1.42 \pm 0.02) \times 10^{-3}\ m$$

also

$$W_V = \left[\left(\frac{\partial V}{\partial Q} W_Q\right)^2 + \left(\frac{\partial V}{\partial d} W_d\right)^2\right]^{1/2}$$

$$= V \times \left[\left(\frac{W_Q}{Q}\right)^2 + \left(-\frac{2W_d}{d}\right)^2\right]^{1/2}$$

which gives $V = (1.45 \pm 0.075)\ m/s$ (±5.2%)

(16) Reynolds Number (Re)

$$Re = \frac{Vd\rho}{\eta}$$

where $V = (1.45 \pm 0.075)$ m/s ($\pm 5.2\%$)

$d = (1.42 \pm 0.02) \times 10^{-3}$ m

$\rho = (998 \pm 16)$ kg/m^3

$\eta = (2.67 \pm 0.17) \times 10^{-3}$ Pa Sec

also

$$W_{Re} = [(\frac{\partial Re}{\partial d} W_d)^2 + (\frac{\partial Re}{\partial V} W_V)^2 + (\frac{\partial Re}{\partial \rho} W_\rho)^2 + (\frac{\partial Re}{\partial \eta} W_\eta)^2]^{1/2}$$

$$= Rex[(\frac{W_V}{V})^2 + (\frac{W_d}{d})^2 + (\frac{W_\rho}{\rho})^2 + (-\frac{W_\eta}{\eta})^2]^{1/2}$$

which gives $Re = 771 \pm 65$ ($\pm 8.4\%$)

(17) Apparent Viscosity obtained from the Rotary Viscometer (Table 3; $\dot{\gamma} = 487.0$)

We have $\eta = \frac{\tau}{\dot{\gamma}} = \frac{(\tau\%)K}{\dot{\gamma}}$

where $\tau\% = 13.6 \pm 1$

$K = 0.2239 \pm 0$

$\dot{\gamma} = 487.0 \pm 0$ sec^{-1}

Here K is a calibration constant supplied for the particular measurement system used.

$$W_\eta = \left[\frac{\eta}{\tau\%} \cdot W_{\tau\%} \right]$$

which gives $\eta = (6.3 \pm 0.5) \times 10^{-3}$ PaS (±7.4%)

VITA AUCTORIS

1958 Born in Kurichi, Coimbatore, India on May 21.

1974 Completed high school at St. Michael's High School, Coimbatore, India in May.

1975 Completed Preuniversity course at P.S.G. College of Arts and Sciences, Coimbatore, India in May.

1980 Received the Degree of Bachelor of Engineering (Honours) in Mechanical Engineering from University of Madras (P.S.G. College of Technology), India in June.

1982 Currently a candidate for the Degree of Master of Applied Science in Mechanical Engineering at the University of Windsor, Windsor, Ontario, Canada.